frontiers in
MICROBIOLOGY

ORIGINAL RESEARCH ARTICLE
published: 22 February 2011
doi: 10.3389/fmicb.2011.00027

Vaccination with human induced pluripotent stem cells creates an antigen-specific immune response against HIV-1 gp160

Shinji Yoshizaki[1], Mayuko Nishi[1], Asami Kondo[1], Yoshitsugu Kojima[1], Naoki Yamamoto[2] and Akihide Ryo[1]*

[1] Department of Microbiology, Yokohama City University Graduate School of Medicine, Yokohama, Kanagawa, Japan
[2] Department of Microbiology, National University of Singapore, Singapore, Singapore

Edited by:
Hironori Sato, National Institute of Infectious Diseases, Japan

Reviewed by:
Masaru Yokoyama, National Institute of Infectious Diseases, Japan
Takao Masuda, Tokyo Medical and Dental University, Japan

***Correspondence:**
Akihide Ryo, Department of Microbiology, Yokohama City University School of Medicine, 3-9 Fuku-ura, Kanazawa-ku, Yokohama, Kanagawa 236-0004, Japan.
e-mail: aryo@yokohama-cu.ac.jp

Induced pluripotent stem cells (iPSCs) are artificially derived from somatic cells that have been transduced with defined reprogramming factors. A previous report has indicated the possibility of using iPSCs as an immune stimulator to generate antigen-specific immunity. In our current study, we have investigated whether human iPSCs (hiPSCs) have the ability to enhance specific immune response against a human immunodeficiency virus type 1 (HIV-1) antigen in a xenogenic mouse model. Our results show that BALB/c mice immunized with hiPSCs transduced with an adenoviral vector encoding HIV-1 gp160 exhibited prominent antigen-specific cellular immune responses. We further found that pre-treatment of hiPSCs with ionizing radiation promotes the secretion of pro-inflammatory cytokines such as interleukin-1 alpha (IL-1α), IL-12, and IL-18. These cytokines might promote the activation of antigen-presenting cells and the effective induction of cellular immunity. Our present findings thus demonstrate that a hiPSCs-based vaccine has the potential to generate cellular immunity against viral antigens such as HIV-1 gp160 in a xenogenic condition.

Keywords: human induced pluripotent stem cells, ionizing radiation, pro-inflammatory cytokine, cellular immunity, vaccine

INTRODUCTION

The latest estimate indicates that 33.4 million people are living with human immunodeficiency virus (HIV)/AIDS in 2009, and there are some 2.7 million new infections each year. Globally, HIV/AIDS is the leading cause of mortality among younger people and children where 2.0 million people die annually. The development of a safe and effective HIV/AIDS vaccine is required urgently to halt this epidemic. There is currently no effective AIDS vaccine available (McElrath and Haynes, 2010).

Current approaches in the development of HIV/AIDS vaccines have focused not on preventing infection itself, but on eliciting potent antiviral-specific $CD8^+$ T cell [cytotoxic T lymphocyte (CTL)] responses to limit viral replication (Yamamoto and Matano, 2008). This is in part because such an immune response contributes to non-progression of AIDS in people infected with HIV type 1 (HIV-1). It is thus desirable to develop a new vaccine vector system for generating effective CTL response against HIV-1.

Recently, reprogramming of human somatic cells into pluripotent embryonic stem (ES) cell-like cells, termed human induced pluripotent stem cells (hiPSCs) has been successfully achieved by the transduction of four defined transcription factors (Klf4, Oct4, Sox2, and c-Myc; Takahashi and Yamanaka, 2006; Takahashi et al., 2007; Park et al., 2008). This technology does not require embryos or oocytes, thereby facilitating the generation of individual-specific pluripotent stem cells that are valuable for personalized cell transplantation therapy without concern for immune rejection.

A recent report has demonstrated a new application of hiPSCs as an immune stimulator. Li et al. (2009b) demonstrated that the inoculation of human ES cells (ESCs) or hiPSCs can induce a protective immune response against murine colon cancer cells. It is considered that the pluripotent stem cell induces the immune response *in vivo* against colon cancer cells expressing oncofetal antigens that are present in normal stem cells (Li et al., 2009b). Moreover, other studies demonstrated that ESCs can produce pro-inflammatory cytokines and growth modulators following a treatment with ionizing radiation (Guo et al., 2006). We therefore hypothesized that irradiated hiPSCs expressing the HIV-1 antigen have a potency to induce the antigen-specific CTL response.

In our current study, we selected HIV-1 gp160 as a model antigen for evaluating the ability of hiPSCs as a vaccine vector. Our current results provide evidence for the capacity of hiPSCs to induce antigen-specific immunity against viral proteins.

MATERIALS AND METHODS

CELL CULTURE

Human induced pluripotent stem cells (hiPSCs) were derived from adult human fibroblasts and were obtained from the RIKEN Bioresource Center (clone no. 201B7; Takahashi et al., 2007). The hiPSCs were cultured on plates coated with Matrigel (BD Biosciences, San Jose, CA, USA) and maintained in Knockout Dulbecco's modified Eagle's medium (Invitrogen, Carlsbad, CA, USA) supplemented with 20% Knockout SR (Invitrogen), 1% GlutaMAX (Invitrogen), 100 μM non-essential amino acids (Invitrogen), 50 μM β-mercaptoethanol, and 10 ng/ml human

Abbreviations: APC, antigen-presenting cell; CAG promoter, CMV enhancer/β-actin promoter with β-actin intron; DsRed, *Discosoma* sp. red fluorescent protein; hiPSC, human induced pluripotent stem cell; HIV, human immunodeficiency virus; IL-1, interleukin-1; MHC, major histocompatibility complex; NF-κB, nuclear factor-κB.

basic fibroblast growth factor (bFGF) and conditioned medium for mouse embryonic fibroblasts. MRC5 (human fetal lung fibroblasts) and RAW 264.7 (mouse monocyte/macrophage) cell lines were maintained in Dulbecco's modified Eagle's medium (DMEM; Wako, Osaka, Japan) supplemented with 10% heat-inactivated fetal bovine serum.

ADENOVIRUS VECTOR

The adenovirus vectors expressing HIV-1 Rev and Env gp160 proteins (Ad-gp160) or *Discosoma* sp. red fluorescent protein (DsRed, Ad-Red) were generated as described previously (Abe et al., 2009). These adenoviral vectors are replication-defective recombinant adenovirus type 5 virus lacking the E1 and E3 regions (Mizuguchi and Kay, 1998). The expression of HIV-1 *rev-env gp160*, or *DsRed* was controlled using the CMV enhancer/β-actin promoter with β-actin intron (CAG promoter). These vectors were propagated in HEK293 cells and purified by two repetitions of the CsCl method as described elsewhere (Lieber et al., 1996). The total concentration of virions in each preparation was calculated from the optical density at 260 nm (OD_{260}), using the formula 1 $OD_{260} = 1 \times 10^{12}$ viral particle (vp)/ml.

ANTIBODIES AND IMMUNOBLOTTING

HiPSCs were transduced with Ad-gp160 or Ad-Red at 3,000 vp/cell for 24 h. The cellular lysates were then subjected to immunoblotting analysis with anti-HIV-1 gp120, anti-HIV-1 gp41 (AIDS Research and Reference Reagent Program, NIH, MD, USA), anti-Oct4 (C-10; Santa Cruz Biotechnology, Santa Cruz, CA, USA), anti-SOX2 (Millipore, Billerica, MA, USA), anti-phosphorylated IκB-α (Active Motif, Carlsbad, CA, USA), anti-IκB-α (Santa Cruz Biotechnology) or anti-β-actin monoclonal antibodies (AC-15; Sigma, Saint Louis, MO, USA). Immunoblotting images were acquired using LAS3000 (Fujifilm, Tokyo, Japan).

FLOW CYTOMETRY ANALYSIS

HiPSCs and MRC5 fibroblasts were harvested with 0.02% EDTA in phosphate buffered saline (PBS), dissociated into single cells, and stained with the fluorescein isothiocyanate (FITC)-conjugated anti-HLA-ABC antibody (W6/32; BioLegend, San Diego, CA, USA). The cells were then analyzed by flow cytometry (FACSCantoII, BD Biosciences). For the evaluation of effector $CD8^+$ T cells, peripheral blood mononuclear cells (PBMCs) from immunized mice were stained with phycoerythrin/cyanin7 (PE-Cy7)-conjugated anti-mouse CD62L (MEL-14; BioLegend) and FITC-conjugated anti-mouse CD8a antibodies (Ly-2; eBioscience, San Diego, CA, USA) without stimulation. The cells were then analyzed by flow cytometry (FACSCantoII). $CD62L^-$ $CD8^+$ T cells were defined as effector $CD8^+$ T cells.

ANIMAL IMMUNIZATION

Generally, to estimate cell-based vaccine, 1×10^5 to 1×10^6 cells were inoculated into a mouse (Yoon et al., 2008; Li et al., 2009a; Senju et al., 2009). We thus introduced 5×10^5 cells in this immunization. We employed immunization protocol described as follows. Eight-week-old female BALB/c mice ($H\text{-}2D^d$) were purchased from Japan SLC Inc. (Shizuoka, Japan) and housed in an animal facility. Under anesthesia, these mice were injected subcutaneously (s.c.) with 5×10^5 15 Gy-irradiated or formalin-fixed (2%, 15 min) hiPSCs expressing either DsRed or HIV-1 gp160, three times at 2- or 4-week intervals. The study was approved by the Animal Administer Community of Yokohama City University.

TETRAMER ASSAY

Tetramer assay is a well-established way to examine the antigen-specific CTL in mouse models (Villacres et al., 2000; Hovav et al., 2007). Peptide 18 (p18: RGPGRAFVTI) derived from the V3 loop of $HIV\text{-}1_{IIIB}$ gp160 is an epitope recognized by CTL in the BALB/c mouse ($H\text{-}2D^d$) model immunized with $HIV\text{-}1_{IIIB}$ gp160 protein (Takahashi et al., 1988). $H\text{-}2D^d$/p18 tetramer was tetrameric $H\text{-}2D^d$ major histocompatibility complex (MHC) class I with the p18 labeled with phycoerythrin (PE) synthesized by NIH Tetramer 116 Core Facility (Atlanta, GA, USA). The number of $CD8^+$ T cells expressing T cell receptor (TCR) that recognized $H\text{-}2D^d$/p18 tetramer was examined by tetramer assay. Tetramer assays were performed using a $H\text{-}2D^d$/p18 tetramer as previously described (Shimada et al., 2010). Briefly, PBMCs were isolated from immunized mice, and stained with a PE-conjugated $H\text{-}2D^d$/p18 tetramer and FITC-conjugated anti-mouse CD8a antibody. The cells were then analyzed by flow cytometry (FACSCantoII).

INTRACELLULAR CYTOKINE STAINING ASSAY

Intracellular cytokine staining (ICS) assays were performed as previously described (Shimada et al., 2010). Briefly, PBMCs were obtained from immunized mice, and the red blood cells were removed using lysing buffer (BD Bioscience). The lymphocytes were incubated with p18 (RGPGRAFVTI) from the V3 loop of $HIV\text{-}1_{IIIB}$ gp160 protein, and treated with BD GolgiStop (BD Bioscience) for 6 h at 37°C. The cells were then stained with FITC-conjugated anti-mouse CD8a antibody, suspended in cytofix/cytoperm solution (BD Bioscience), and incubated with the PE-conjugated anti-mouse interferon-gamma (IFN-γ) antibody (XMG1.2; eBioscience). The cells were subsequently analyzed by flow cytometry (FACSCantoII) utilizing FACSDiva software.

RT-PCR

Total RNA was isolated by TRIzol reagent (Invitrogen), and reverse-transcribed using ReverTra Ace (Toyobo, Osaka, Japan) in accordance with the manufacturer's instructions. The resulting cDNAs were amplified with Ex Taq DNA polymerase (Takara Bio, Otsu, Japan). To quantify the cytokine RNA levels, a SYBR premix Ex Taq II (Takara Bio) was used and analyses were performed using the ABI PRISM Sequence Detector System 7500 (Applied Biosystems, Foster City, CA, USA). The primer sets used for RT-PCR were as follows: *interleukin (IL)-1α*: 5′-tcgagccaatgatcagtacc-3′ and 5′-tggtctcactacctgtgatg-3′; *IL-18*: 5′-gaccaagttctcttcattgacc-3′ and 5′-tgtcctgggacacttctctg-3′; *IL-12A*: 5′-atgatggccctgtgccttag-3′ and 5′-gtggcacagtctcactgttg-3′; *Oct4*: 5′-gagatatgcaaagcagaaacc-3′ and 5′-cttcactgcactgtactcct-3′; *Nanog*: 5′-atggttggagcctaatcagc-3′ and 5′-tgttgtccttagcagccaag-3′; *hTERT*: 5′-ccgtacatgcgacagttcg-3′ and 5′-caagaaatcatccaccaaacg-3′, and *glyceraldehydes-3-phospate dehydrogenase* (*gapdh*): 5′-ccatggagaaggctgggg-3′ and 5′-caaagttgtcatggatgacc-3′. The *IL-1α*, *IL-18*, or *IL-12A* transcripts were normalized using the *gapdh* expression levels, and analyzed by the comparative C_T method.

ENZYME-LINKED IMMUNOSORBENT ASSAY

The culture supernatants were collected from the irradiated hiPSCs at 24-h post-irradiation, centrifuged to remove cellular debris prior to filtration, and then subjected to enzyme-linked immunosorbent assay (ELISA) in accordance with the manufacturer's instructions (R&D Systems, Minneapolis, MN, USA).

ACTIVATION OF MOUSE SPLENOCYTES WITH hiPSCs

Activation of mouse splenocytes with hiPSCs was detected by the co-culture system. Generally, the cell-to-cell co-culture system employs from 1:1 to 1:10 in the ratio of effector cells to target cells in number (Maitra et al., 2004; Hall et al., 2008). HiPSCs (2×10^5 cells) were co-cultured with mouse splenocytes (2×10^6 cells) from naive mouse, at a ratio of 1:10. We employed the assay protocol described previously (Yoon et al., 2008). In brief, 200,000 hiPSCs were treated by either 15 Gy-irradiation or 2% formalin solution for 15 min, and then co-cultured or cultured in transwells (pore size, 0.4 μm) with 2×10^6 BALB/c mouse splenocytes for 40 h. The splenocytes were then stained with FITC-anti-mouse CD11c (HL3; BD Bioscience) and PE-anti-mouse CD86 (PO.3; eBioscience) or PE-anti-mouse MHC class II antibodies (M5/114.15.2; eBioscience). The cells were analyzed under flow cytometry (FACSCantoII) utilizing FACSDiva version 6.1.2 software.

MICROARRAY ANALYSIS

Total RNAs for microarray analysis were isolated from hiPSCs cultured at 14 h post-irradiation with TRIzol (Invitrogen) and then analyzed using the Affymetrix GeneChip Human Genome U133 Plus 2.0 Array and GeneChip Scanner 3000. The gene expression levels were compared between irradiated hiPSCs and the non-treated control hiPSCs. Up-regulated genes showing at least a two-fold change were identified using DNA MicroArray Viewer Software (Kurabo, Osaka, Japan).

MEASUREMENT OF NUCLEAR FACTOR-KAPPA B ACTIVATION

The culture supernatant was recovered from the irradiated hiPSCs at 24-h post-irradiation. To neutralize IL-1α in the culture supernatant, anti-human-IL-1α-neutralizing antibody (PeproTech, Rocky Hill, NJ, USA) or rabbit sera as control were added at 0.1 or 1 μg/ml. Two hours after incubation, RAW 264.7 cells were incubated with the culture supernatants for 10 min. Cell lysates were then immunoblotted with anti-phosphorylated IκB-α (Active Motif) or anti-IκB-α antibodies (Santa Cruz Biotechnology).

STATISTICAL ANALYSES

We performed the experiment with $n = 3$. All values are expressed as mean ± error. Statistical analyses were performed using Mann–Whitney's *U*-test with StatView 5.0 software (SAS Institute Inc., Cary, NC, USA), and $P < 0.05$ was considered to be statistically significant.

RESULTS

TRANSDUCTION OF UNDIFFERENTIATED HUMAN iPSCs WITH AN ADENOVIRUS VECTOR EXPRESSING HIV-1 gp160

We initially investigated the efficient gene transfer into hiPSCs. Previous reports indicated that the CAG-promoter-driven adenoviral vector system can effectively transduce genes into hiPSCs without aberrant cell differentiation (Tashiro et al., 2010). We thus utilized a replication-defective human adenovirus type 5 vector encoding either HIV-1 gp160 (Ad-gp160) or DsRed (Ad-Red) under the control of the CAG promoter. We detected the successful expression of HIV-1 gp160 in hiPSCs by immunoblotting with either anti-HIV-1 gp41 or anti-HIV-1 gp120 antibodies (**Figure 1A**). Flow cytometric analysis further revealed that >90 and 60% of the transduced hiPSC population expressed DsRed and HIV-1 gp160, respectively (**Figure 1B**).

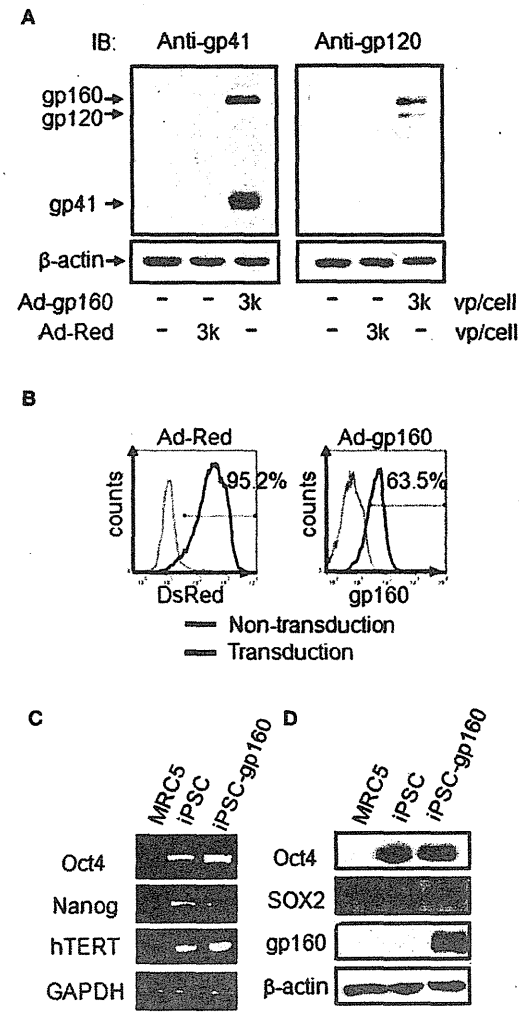

FIGURE 1 | Expression of HIV-1 gp160 in hiPSCs. (A,B) hiPSCs were transduced with adenoviral vectors encoding HIV-1 gp160 (3,000 vp/cell) or DsRed (3,000 vp/cell) for 24 h. The HIV-1 gp160 protein and its cleaved product (gp41 and gp120) were detected by immunoblotting against anti-HIV-1 gp41 [**(A)** left] or anti-HIV-1 gp120 antibodies [**(A)** right]. β-actin was used as the internal control. The expression of DsRed or HIV-1 gp160 protein was measured by flow cytometry **(B)**. The staining patterns of transduced (thick line) and non-transduced (thin line) cells are shown. Percentages of positive-cells after transduction with each adenoviral vectors are also indicated. **(C)** iPSC markers (Oct4, Nanog, and hTERT) and GAPDH mRNAs were detected in, MRC5 fibroblasts, non-transduced hiPSCs or Ad-gp160-transduced hiPSCs at 24 h by RT-PCR. **(D)** The iPSC markers Oct4 and SOX2, and HIV-1 gp160 proteins were detected by immunoblotting of MRC5 fibroblasts, non-transduced hiPSCs, and Ad-gp160-transduced hiPSCs.

We next addressed whether hiPSCs would retain their pluripotency following the transduction of exogenous genes. RT-PCR analysis revealed that the iPSC markers Oct4, Nanog, and hTERT were strongly expressed in the cells before and after the transduction of HIV-1 gp160, but this was not the case in MRC5 fibroblasts (**Figure 1C**). Moreover, the protein expression of Oct4 and SOX2 was also detectable in Ad-infected hiPSCs during immunoblotting analysis (**Figure 1D**).

IMMUNIZATION WITH hiPSCs AND THE IMMUNE RESPONSES GENERATED

We investigated whether hiPSCs could induce cellular immune response against the viral antigen in a mouse model. Before immunization, flow cytometric analysis confirmed that hiPSCs expressed an extremely low level of MHC class I as compared with MRC5 fibroblasts on cell surfaces (**Figure 2A**), suggesting the minimum xenogenic reaction in a mouse inoculated with hiPSCs.

We next generated a formalin-fixed and irradiated hiPSCs-based vaccine expressing HIV-1 gp160. Because cell differentiation can be paralleled with cell proliferation as asymmetric cell division (Morrison and Kimble, 2006), the formalin-fixation or irradiation can abrogate both cell growth and differentiation (**Figure 2B**). To examine whether hiPSCs expressing HIV-1 gp160 could stimulate an immune response, we immunized immunocompetent BALB/c mice with either formalin-fixed or irradiated hiPSCs expressing HIV-1 gp160 (hiPSCs-gp160) or DsRed (hiPSCs-Red). These mice were boosted twice on days 15 and 40 (**Figure 2C**). In this protocol, the immunized mice did not show any clinical signs of adverse effects accompanied by xenogenic immune reaction such as skin rash, arthritis, or overt organ dysfunction (data not shown). On days 0, 7, 22, and 47 after the first immunization, we performed the well-established H-2D^d/p18 tetramer-binding assay. P18 (RGPGRAFVTI) is an epitope recognized by CTL in BALB/c mouse (H-2D^d) model immunized with HIV-1_{IIIB} gp160 protein (Takahashi et al., 1988). This assay measures CD8$^+$ T cells recognizing the H-2D^d-restricted p18 derived from the V3 loop of the HIV-1_{IIIB} gp160 protein. At the same time, we conducted an ICS assay to detect cellular IFN-γ expression following stimulation with the p18. The results showed that p18 antigen-specific CD8$^+$ T lymphocytes were substantially induced in mice injected with irradiated hiPSCs-gp160 as compared with other groups. It was statistically significant on Day 47 (**Figure 2D**). Although boost effects such as clonal expansion of p18-specific CD8$^+$ T cells were not observed in mice after booster immunization with the hiPSC-based vaccine, antigen-specific IFN-γ-producing CD8$^+$ T lymphocytes were significantly increased up to 47 days in mice immunized with irradiated hiPSCs-gp160 further than the other groups (**Figure 2E**). Moreover, the proportion of total effector CD8$^+$ T lymphocytes (CD62L$^-$ CD8$^+$ cells) was also found to be substantially increased by the immunization with irradiated hiPSCs-gp160 (**Figure 2F**).

We next examined the induction of HIV-1 gp160-specific antibodies in the sera from immunized mice by immunoblotting. We tested the immunoreactivity of the sera against cell lysates from either control 293T cells or those expressing HIV-1 gp160. We found that sera from mice immunized with formalin-fixed hiPSCs-gp160 contained antibodies that targeted the HIV-1 gp160 protein and its cleavage product, gp41, whereas this was not the case for the sera from mice injected with irradiated hiPSCs (**Figure 2G**). Furthermore, the sera from mice immunized with formalin-fixed hiPSCs-gp160 but not with irradiated hiPSCs, contained antibodies against cell surface antigens of hiPSCs itself as revealed by flow cytometry (**Figure 2H**).

These results indicate that formalin-fixed hiPSCs-gp160-immunized mice were induced with antibodies against HIV-1 gp160 and against cell surface antigens of hiPSCs. The latter antibodies have the potential to rapidly eradicate hiPSCs-based vaccines during immunization in mice. Whereas, irradiated hiPSCs induced more antigen-specific CD8$^+$ T cells than formalin-fixed hiPSCs and less antibody against hiPSCs.

IRRADIATED hiPSCs STIMULATE CD11c$^+$ SPLENOCYTES THROUGH A CONTACT-INDEPENDENT MECHANISM USING SOLUBLE MOLECULES

We next addressed whether irradiated hiPSCs could modulate the activity and function of immune cells such as antigen-presenting cells (APCs). Splenocytes from a BALB/c mouse were co-cultured with either formalin-fixed hiPSCs or irradiated hiPSCs, and then examined by flow cytometry for the expression of the activation marker CD86 or MHC class II in CD11c$^+$ cells. Upon co-culture with irradiated hiPSCs, but not with formalin-fixed cells, the expression levels of both CD86 and MHC class II were significantly increased in the CD11c$^+$ cell population (**Figures 3A,B**).

To further investigate whether the stimulatory effects of irradiated hiPSCs upon CD11c$^+$ cells were dependent on cell-to-cell interactions or soluble factors, transwell experiments were performed. HiPSCs and mouse splenocytes were separately cultured in the lower and upper chambers of a transwell, and then analyzed for the expression of activation markers on CD11c$^+$ cell. Our results showed that these activation markers were indeed induced in the transwell system in a similar manner to the co-culture system (**Figures 3C,D**). We thus concluded that soluble factors from irradiated hiPSCs play a role in their stimulatory effects upon CD11c$^+$ cells.

INDUCTION OF PRO-INFLAMMATORY CYTOKINES IN hiPSCs BY RADIATION

To identify the soluble factors that are secreted from irradiated hiPSCs, we performed a DNA microarray experiment to screen for ionizing radiation-induced factors in these cells. Total RNAs extracted from irradiated or untreated hiPSCs were subjected to DNA microarray analysis. Following data normalization, we selected genes that were induced more than two-fold upon exposure to ionizing radiation (**Figure 4A**). We found that multiple cytokines were up-regulated in hiPSCs by ionizing radiation. In particular, pro-inflammatory cytokine IL-1α and T helper type 1 (Th1)-related cytokines IL-12A and IL-18 were prominently induced under these conditions. The expression of these cytokines was further analyzed by either conventional RT-PCR or quantitative RT-PCR (qPCR). Consistent with the microarray data, IL-1α, IL-12A, and IL-18 genes were found to be significantly increased at 24 h after irradiation (5.00-, 2.50-, and 2.46-fold, respectively; **Figures 4B,C**). Notably, the expression of these cytokines was not induced by an adenovirus infection (data not shown). We next investigated whether the cytokines production/induction was observed in MRC5 fibroblasts following ionizing irradiation. We found that there was little induction of IL-12A and IL-18 following the irradiation. Furthermore,

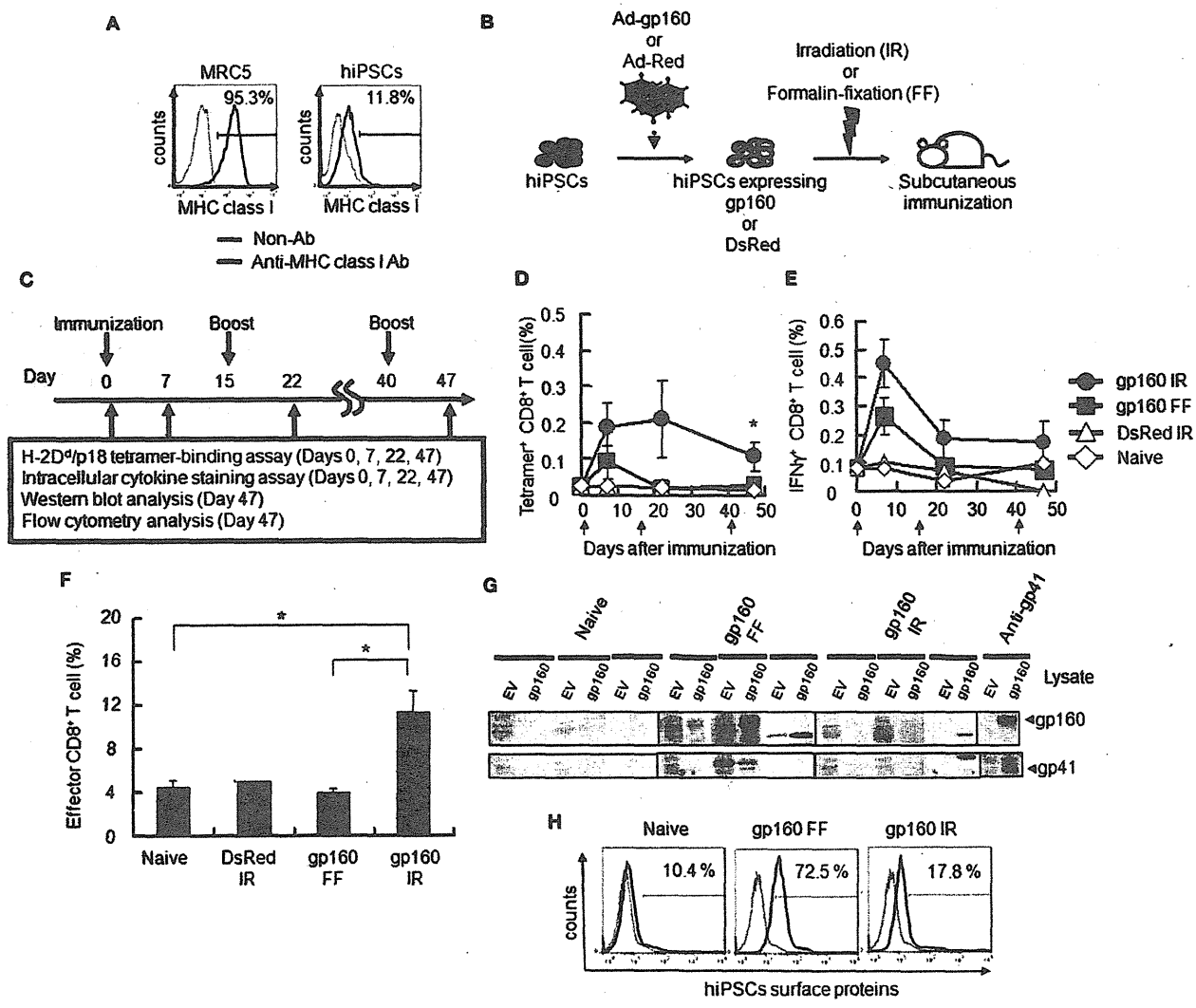

FIGURE 2 | Antigen-specific immunity in mice immunized with hiPSCs expressing gp160. (A) MRC5 fibroblasts and hiPSCs were stained with the anti-HLA-ABC antibody followed by flow cytometry. Note that MHC class I expression in hiPSCs was extremely low compared with MRC5. **(B)** Pre-treatment of hiPSCs before vaccination. hiPSCs were infected with adenoviral vector encoding either HIV-1 gp160 or DsRed before inoculation. Cells were then irradiated with 15 Gy or fixed with 2% formalin solution prior to the vaccination **(C)** This diagram indicates a protocol for mouse immunization with hiPSCs. **(D,E)** Female BALB/c mice (8–10 weeks old) were inoculated s.c. with PBS, 5×10^5 formalin-fixed hiPSCs-gp160 (gp160 FF), irradiated hiPSCs-gp160 (gp160 IR) or irradiated hiPSCs-Red (DsRed IR) and then boosted twice with the same cell groups on days 15 and 40 after the first immunization. Antigen-specific CD8$^+$T lymphocytes were measured via a H-2D^d/p18 tetramer-binding assay **(D)**. PBMCs from immunized mice were stimulated with the p18 peptide derived from the V3 loop of HIV-1 gp160 and then treated with BD Golgistop for 6 h. HIV-specific IFN-γ-producing CD8$^+$T lymphocytes were measured by flow cytometry with anti-CD8a-FITC and anti-IFNγ-PE **(E)**. Arrows indicate the day of immunization. **(F)** PBMCs were collected 7 days after the first immunization and stained with anti-CD62L-PE-Cy7 and anti-CD8a-FITC antibodies without stimulation. Effector CD8$^+$T lymphocytes (CD62L$^-$ CD8$^+$) were measured by flow cytometry. **(G)** Immunoblotting analysis with immunized mouse sera against total cell lysates from 293T cells transfected with empty vector (EV) or HIV-1 gp160 expressing plasmid. **(H)** Non-permeabilized hiPSCs were stained with pooled sera from mice immunized with formalin-fixed or irradiated hiPSCs-gp160 and then stained with FITC-anti-mouse immunoglobulin G (IgG) antibody followed by flow cytometry. Staining patterns obtained for the pooled sera (thick line) or control (thin line) are shown. All data are the mean ± error of three mice per group. $^*P < 0.05$.

MRC5 fibroblasts did not express IL-1α irrespective of the irradiation (**Figure 4D**). These results indicate that hiPSCs can efficiently produce these cytokines after irradiation.

We next examined the cytokine production levels from irradiated hiPSCs. Culture supernatants from these cells were collected and analyzed by ELISA. We found a substantial increase in the IL-1α level upon irradiation (**Figure 4E**), whereas IL-12 and IL-18 were not detectable by ELISA (data not shown). We further analyzed the biological function of IL-1α secreted from irradiated hiPSCs to mouse immune cells using a mouse monocyte/macrophage cell line RAW 264.7. Activation of RAW 264.7 was monitored by measuring of IκB-α phosphorylation. Cell supernatants from irradiated

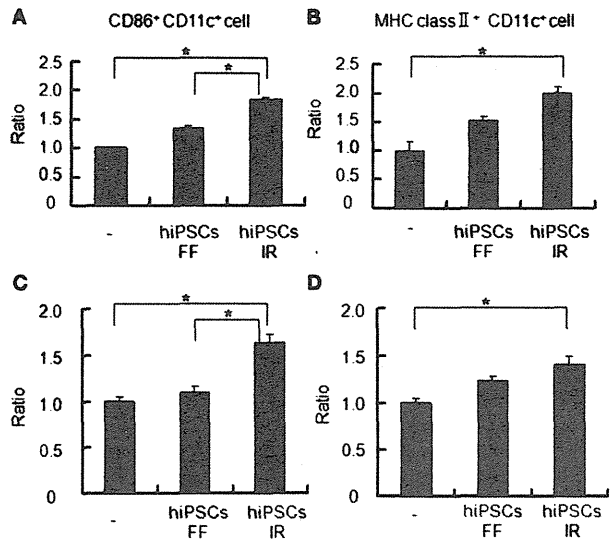

FIGURE 3 | Activation of mouse APCs by hiPSCs. (A,B) BALB/c mouse splenocytes were co-cultured with or without formalin-fixed (FF) or irradiated (IR) hiPSCs for 40 h, and the relative expression of CD86 **(A)** and MHC class II proteins **(B)** on the cell surface of CD11c+ splenocytes was monitored by flow cytometry. **(C,D)** BALB/c mouse splenocytes were seeded on transwell filters (0.4 μm pore) and co-cultured with irradiated or formalin-fixed hiPSCs in the bottom compartments for 40 h. The relative expression of CD86 **(C)** and MHC class II **(D)** was then monitored by flow cytometry. $*P < 0.05$.

hiPSCs, but not control supernatant, significantly induced the phosphorylation of IκB-α, indicative of nuclear factor-kappa B (NF-κB) activation (**Figure 4F**). A neutralizing antibody against IL-1α, but not control serum, was found to suppress this phosphorylation of IκB-α (**Figure 4F**), demonstrating that IL-1α from irradiated hiPSCs can activate NF-κB signaling in RAW 264.7 cells. These results indicate that ionizing radiation can effectively induce the production of IL-1α in hiPSCs for the activation of APCs and the antigen-specific immune responses.

DISCUSSION

Our present findings uncover a novel function of hiPSCs in the generation of viral antigen-specific immune responses as a cell-based vaccine. We found from our analyses that (1) Adenovirus system can effectively introduce exogenous viral antigen in hiPSCs without aberrant cell differentiation; (2) Radiation treatment can efficiently induce the cytokine production of IL-1α, IL-12, and IL-18; and (3) Inoculation of irradiated hiPSCs can enhance the antigen-specific cellular immune response even in xenogenic condition. These results indicate that hiPSCs can promote cellular immunity against an exogenously expressed viral antigen in a xenogenic condition.

We utilized the adenoviral vector system to express exogenous viral antigen in hiPSCs. Adenovirus has been shown previously to effectively transfer exogenous genes into hiPSCs (Tashiro et al., 2010) and we obtained a high efficiency in this regard without any effects upon cell differentiation. Moreover, >75% of the cells survived the adenoviral transduction which typically causes a reasonable amount of cell death in primary cultures (data not shown). Thus the adenoviral vector system is suitable for use with hiPSCs owing to its high transduction efficiency and low cellular toxicity.

Our current immunization protocol demonstrated that the boost stimulation with irradiated hiPSCs-gp160 did not induce the clonal expansion of antigen-specific $CD8^+$ T cells. Unlike the vaccine model with viral vectors, boost effects are usually not obvious in cell-based vaccines (Li et al., 2009a). However, a boost stimulation can prolong the long-standing immune response against antigens. Consistently, our current hiPSCs vaccine system can induce relatively high levels of antigen-specific $CD8^+$ T cells in the long term. This could be an advantage of the hiPSCs-based vaccine although further analytical and experimental studies are required to better understand and evaluate the vaccine system.

The immunization of mice with irradiated hiPSCs causes the induction of cellular immunity rather than humoral immunity, which is in contrast to the result of immunization with formalin-fixed hiPSCs. Previous studies have suggested that Th1- and Th2-cells direct different immune response pathways (Kidd, 2003). Our present data indicates that irradiated hiPSCs may induce Th1-cytokines that contribute to the Th1 shift in immunized mice resulting in the induction of antigen-specific CTL. Furthermore, pre-treatment with ionizing radiation could reduce the generation of antibodies against the hiPSC vector itself. Thus, ionizing irradiation might be a proper procedure in the hiPSCs-based vaccine system.

In our current study, we evaluated the ability of hiPSCs to induce antigen-specific CTL as a cell-based vaccination in a xenogenic mouse model. In fact, a previous report presented by Li et al. (2009b) demonstrates that hiPSCs can produce a tumor antigen-specific immune reaction leading to a tumor rejection even in a xenogenic condition. It has been reported that MHC molecules could strongly induce xenogenic immune reactions. As we and others have revealed, hiPSCs express a very low level of MHC molecules on the cell surface (Suarez-Alvarez et al., 2010). With this knowledge in hand, we decided to use the mouse model of HIV-1 gp160 to assess the ability of hiPSCs as a cell-based vaccine vector. However, it is necessary to investigate the involvement of the xenogenic condition in the antigen-specific immune reaction by the iPSCs-mediated vaccination.

We investigated the MHC-restricted immune response in the xenogenic mouse model in this report. It is likely that inoculated hiPSCs could be phagocytosed by mouse APCs such as dendritic cells followed by the antigen presentation and MHC-restricted immune activation in an immunized mouse. However, a previous report indicates that pluripotent stem cells such as ESCs or iPSCs may have a new system for antigen presentation since these cells express very low level of MHC molecules on their cell surface (Li et al., 2009b). Further experimental studies are necessary for a better understanding of the nature of iPSC as a new type of vaccine vector.

Cytokines are important signaling molecules that mediate communicative interactions both locally and between different cells *in vivo*. We have shown in our present study that irradiation of hiPSCs can selectively induce pro-inflammatory and Th1-related cytokines such as IL-1α, IL-12, and IL-18. Significantly, this was not the case in MRC5 fibroblasts. Cytokine production from irradiated hiPSCs might promote the activation of APCs thereby enhancing cellular immunity against loaded antigen. IL-1α has been shown to be a potent pro-inflammatory cytokine and directly

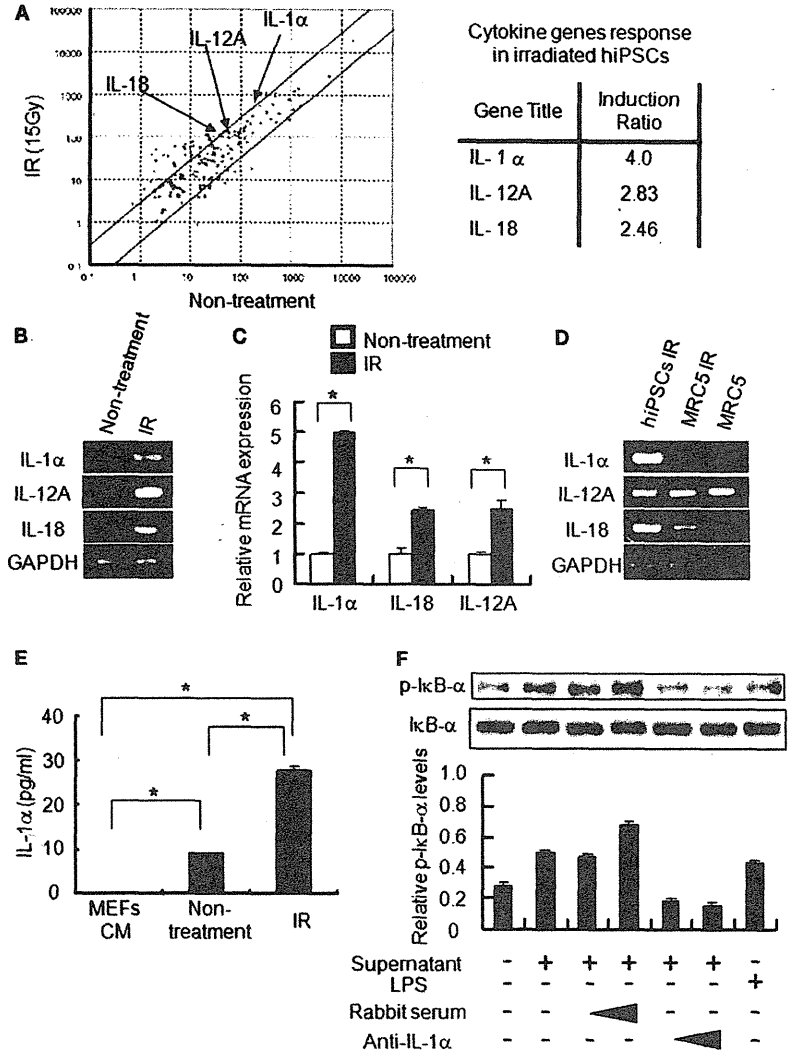

FIGURE 4 | Expression of immune-modulating cytokines in irradiated hiPSCs. (A) A scattered plot comparing the cytokine gene expression profiles of untreated and 15 Gy-irradiated hiPSCs (IR) . Arrows indicate the expression levels of IL-1α, IL-12A, and IL-18. The lines indicate the two-fold changes between the samples. **(B,C)** HiPSCs were either treated or not treated with 15 Gy ionizing radiation. Twenty-four hours later, total RNAs were isolated from untreated or irradiated hiPSCs followed by conventional RT-PCR **(B)** or quantitative RT-PCR (qPCR) **(C)**. Data is normalized to the *gapdh* mRNA levels and represent the mean ± error of three independent experiments. $^*P < 0.05$. **(D)** MRC5 fibroblasts and hiPSCs were either untreated or treated with ionizing radiation (15 Gy). After 24 h, total RNAs were extracted and subjected to RT-PCR analysis for IL-1α, IL-12A, IL-18, and GAPDH. **(E)** Cell culture supernatants were collected from untreated or irradiated hiPSCs followed by IL-1α ELISA. Conditioned media from mouse embryonic fibroblasts (CM-MEFs) was used as a control. **(F)** Filtered culture supernatants from hiPSCs were premixed with rabbit anti-human IL-1α-neutralizing antibody or control rabbit sera for 2 h. RAW 264.7 cells were then exposed to these mixtures (culture supernatant and antibody) for 10 min before preparing whole cell lysates for immunoblotting analysis with either anti-phosphorylated IκB-α (*p*-IκB-α) or anti-IκB-α antibodies. Lipopolysaccharide (LPS) was used as a positive control.

up-regulate NF-κB signaling resulting in the activation of dendritic cells and macrophages (Ardeshna et al., 2000; Yoshimura et al., 2003; Weber et al., 2010). Although much progress has been made in dissecting the complexity of the cytokine network, the role of cytokines from pluripotent stem cells has not been well characterized. Our current results indicate however that the secretion of pro-inflammatory cytokines from hiPSCs might activate APCs via NF-κB activation to accelerate the induction of antigen-specific immune responses *in vivo*. Consistently, previous reports suggest the potent cross-reactivity of human IL-1α and IL-18 to stimulate mouse immune cells whereas the stimulatory effect of human IL-12 p35/p40 hetero-dimer to mouse cells has shown itself to be very marginal (Libert et al., 1990; Schoenhaut et al., 1992; Kong and Li, 2002). Although the precise molecular pathways underlying effective immune responses by hiPSCs have not been investigated, the irradiation-induced modulation of the cytokine expression in these stem cells might confer an effective adjuvant effect during the vaccination processes.

In this report, we evaluated the immunogenicity of hiPSCs which expressed viral antigen in a mouse model. In the future, it is necessary to examine the potency of iPSCs in syn- or allogenic conditions using murine iPSCs. Additionally, the immunogenicity of non-iPSCs should be investigated in comparison with that of iPSCs. However, at least, even in the xenogenic condition, irradiated hiPSCs expressing HIV-1 gp160 protein could induce antigen-specific cellular immune response. Our current results thus provide evidence for the capacity of hiPSCs to induce antigen-specific immunity against the viral proteins.

ACKNOWLEDGMENTS

We thank the RIKEN BioResource Center (Ibaraki, Japan) for providing hiPSCs and MRC5 fibroblasts, the NIH Tetramer Core Facility (Atlanta, GA, USA) for providing tetramers and AIDS Research and Reference Reagent Program for antibodies. We also appreciate Dr. H Mizuguchi for donating the adenoviral vector, and Dr. M Shimada for critical reading of the manuscript. This work was partially supported by grants from Takeda Science Foundation, Uehara Memorial Foundation, and Kanagawa Nanbyo foundation to Akihide Ryo, and an Ishidsu Shun Memorial Scholarship to Shinji Yoshizaki.

REFERENCES

Abe, S., Okuda, K., Ura, T., Kondo, A., Yoshida, A., Yoshizaki, S., Mizuguchi, H., Klinman, D., and Shimada, M. (2009). Adenovirus type 5 with modified hexons induces robust transgene-specific immune responses in mice with pre-existing immunity against adenovirus type 5. *J. Gene Med.* 11, 570–579.

Ardeshna, K. M., Pizzey, A. R., Devereux, S., and Khwaja, A. (2000). The PI3 kinase, p38 SAP kinase, and NF-kappaB signal transduction pathways are involved in the survival and maturation of lipopolysaccharide-stimulated human monocyte-derived dendritic cells. *Blood* 96, 1039–1046.

Guo, Y., Graham-Evans, B., and Broxmeyer, H. E. (2006). Murine embryonic stem cells secrete cytokines/growth modulators that enhance cell survival/anti-apoptosis and stimulate colony formation of murine hematopoietic progenitor cells. *Stem Cells* 24, 850–856.

Hall, B. M., Robinson, C. M., Plain, K. M., Verma, N. D., Carter, N., Boyd, R. A., Tran, G. T., and Hodgkinson, S. J. (2008). Studies on naive CD4 + CD25 + T cells inhibition of naive CD4 + CD25 – T cells in mixed lymphocyte cultures. *Transpl. Immunol.* 18, 291–301.

Hovav, A. H., Cayabyab, M. J., Panas, M. W., Santra, S., Greenland, J., Geiben, R., Haynes, B. F., Jacobs, W. R. Jr., and Letvin, N. L. (2007). Rapid memory CD8+ T-lymphocyte induction through priming with recombinant *Mycobacterium smegmatis*. *J. Virol.* 81, 74–83.

Kidd, P. (2003). Th1/Th2 balance: the hypothesis, its limitations, and implications for health and disease. *Altern. Med. Rev.* 8, 223–246.

Kong, J., and Li, Y. C. (2002). Upregulation of interleukin-18 expression in mouse primary keratinocytes induced to differentiate by calcium. *Arch. Dermatol. Res.* 294, 370–376.

Li, B., Simmons, A., Du, T., Lin, C., Moskalenko, M., Gonzalez-Edick, M., VanRoey, M., and Jooss, K. (2009a). Allogeneic GM-CSF-secreting tumor cell immunotherapies generate potent anti-tumor responses comparable to autologous tumor cell immunotherapies. *Clin. Immunol.* 133, 184–197.

Li, Y., Zeng, H., Xu, R. H., Liu, B., and Li, Z. (2009b). Vaccination with human pluripotent stem cells generates a broad spectrum of immunological and clinical responses against colon cancer. *Stem Cells* 27, 3103–3111.

Libert, C., Brouckaert, P., Shaw, A., and Fiers, W. (1990). Induction of interleukin 6 by human and murine recombinant interleukin 1 in mice. *Eur. J. Immunol.* 20, 691–694.

Lieber, A., He, C. Y., Kirillova, I., and Kay, M. A. (1996). Recombinant adenoviruses with large deletions generated by Cre-mediated excision exhibit different biological properties compared with first-generation vectors *in vitro* and *in vivo*. *J. Virol.* 70, 8944–8960.

Maitra, B., Szekely, E., Gjini, K., Laughlin, M. J., Dennis, J., Haynesworth, S. E., and Koc, O. N. (2004). Human mesenchymal stem cells support unrelated donor hematopoietic stem cells and suppress T-cell activation. *Bone Marrow Transplant.* 33, 597–604.

McElrath, M. J., and Haynes, B. F. (2010). Induction of immunity to human immunodeficiency virus type-1 by vaccination. *Immunity* 33, 542–554.

Mizuguchi, H., and Kay, M. A. (1998). Efficient construction of a recombinant adenovirus vector by an improved *in vitro* ligation method. *Hum. Gene Ther.* 9, 2577–2583.

Morrison, S. J., and Kimble, J. (2006). Asymmetric and symmetric stem-cell divisions in development and cancer. *Nature* 441, 1068–1074.

Park, I. H., Zhao, R., West, J. A., Yabuuchi, A., Huo, H., Ince, T. A., Lerou, P. H., Lensch, M. W., and Daley, G. Q. (2008). Reprogramming of human somatic cells to pluripotency with defined factors. *Nature* 451, 141–146.

Schoenhaut, D. S., Chua, A. O., Wolitzky, A. G., Quinn, P. M., Dwyer, C. M., McComas, W., Familletti, P. C., Gately, M. K., and Gubler, U. (1992). Cloning and expression of murine IL-12. *J. Immunol.* 148, 3433–3440.

Senju, S., Haruta, M., Matsunaga, Y., Fukushima, S., Ikeda, T., Takahashi, K., Okita, K., Yamanaka, S., and Nishimura, Y. (2009). Characterization of dendritic cells and macrophages generated by directed differentiation from mouse induced pluripotent stem cells. *Stem Cells* 27, 1021–1031.

Shimada, M., Yoshizaki, S., Jounai, N., Kondo, A., Ichino, M., Ryo, A., and Okuda, K. (2010). DNA vaccine expressing HIV-1 gp120/immunoglobulin fusion protein enhances cellular immunity. *Vaccine* 28, 4920–4927.

Suarez-Alvarez, B., Rodriguez, R. M., Calvanese, V., Blanco-Gelaz, M. A., Suhr, S. T., Ortega, F., Otero, J., Cibelli, J. B., Moore, H., Fraga, M. F., and Lopez-Larrea, C. (2010). Epigenetic mechanisms regulate MHC and antigen processing molecules in human embryonic and induced pluripotent stem cells. *PLoS ONE* 5, e10192. doi: 10.1371/journal.pone.0010192

Takahashi, H., Cohen, J., Hosmalin, A., Cease, K. B., Houghten, R., Cornette, J. L., DeLisi, C., Moss, B., Germain, R. N., and Berzofsky, J. A. (1988). An immunodominant epitope of the human immunodeficiency virus envelope glycoprotein gp160 recognized by class I major histocompatibility complex molecule-restricted murine cytotoxic T lymphocytes. *Proc. Natl. Acad. Sci. U.S.A.* 85, 3105–3109.

Takahashi, K., Tanabe, K., Ohnuki, M., Narita, M., Ichisaka, T., Tomoda, K., and Yamanaka, S. (2007). Induction of pluripotent stem cells from adult human fibroblasts by defined factors. *Cell* 131, 861–872.

Takahashi, K., and Yamanaka, S. (2006). Induction of pluripotent stem cells from mouse embryonic and adult fibroblast cultures by defined factors. *Cell* 126, 663–676.

Tashiro, K., Kawabata, K., Inamura, M., Takayama, K., Furukawa, N., Sakurai, F., Katayama, K., Hayakawa, T., Furue, M. K., and Mizuguchi, H. (2010). Adenovirus vector-mediated efficient transduction into human embryonic and induced pluripotent stem cells. *Cell. Reprogram.* 12, 501–507.

Villacres, M. C., Zuo, J., and Bergmann, C. C. (2000). Maintenance of CD8(+) T-cell memory following infection with recombinant sindbis and vaccinia viruses. *Virology* 270, 54–64.

Weber, A., Wasiliew, P., and Kracht, M. (2010). Interleukin-1 (IL-1) pathway. *Sci. Signal.* 3, cm1.

Yamamoto, H., and Matano, T. (2008). Anti-HIV adaptive immunity: determinants for viral persistence. *Rev. Med. Virol.* 18, 293–303.

Yoon, T. J., Kim, J. Y., Kim, H., Hong, C., Lee, H., Lee, C. K., Lee, K. H., Hong, S., and Park, S. H. (2008). Anti-tumor immunostimulatory effect of heat-killed tumor cells. *Exp. Mol. Med.* 40, 130–144.

Yoshimura, S., Bondeson, J., Brennan, F. M., Foxwell, B. M., and Feldmann, M. (2003). Antigen presentation by murine dendritic cells is nuclear factor-kappa B dependent both *in vitro* and *in vivo*. *Scand. J. Immunol.* 58, 165–172.

Conflict of Interest Statement: The authors declare that the research was conducted in the absence of any commercial or financial relationships that could be construed as a potential conflict of interest.

Received: 06 January 2011; paper pending published: 11 January 2011; accepted: 04 February 2011; published online: 22 February 2011.

Citation: Yoshizaki S, Nishi M, Kondo A, Kojima Y, Yamamoto N and Ryo A (2011) Vaccination with human induced pluripotent stem cells creates an antigen-specific immune response against HIV-1 gp160. Front. Microbio. 2:27. doi: 10.3389/fmicb.2011.00027

This article was submitted to Frontiers in Virology, a specialty of Frontiers in Microbiology.

OPEN ACCESS Freely available online

PLoS one

Thymic Alterations in GM2 Gangliosidoses Model Mice

Seiichi Kanzaki[1], Akira Yamaguchi[1]*, Kayoko Yamaguchi[1], Yoshitsugu Kojima[2], Kyoko Suzuki[3], Noriko Koumitsu[1], Yoji Nagashima[1], Kiyotaka Nagahama[1], Michiko Ehara[1], Yoshio Hirayasu[3], Akihide Ryo[2], Ichiro Aoki[1], Shoji Yamanaka[1]

1 Department of Pathology, Yokohama City University School of Medicine, Yokohama, Japan, 2 Department of Microbiology, Yokohama City University School of Medicine, Yokohama, Japan, 3 Department of Psychiatry, Yokohama City University School of Medicine, Yokohama, Japan

Abstract

Background: Sandhoff disease is a lysosomal storage disorder characterized by the absence of β-hexosaminidase and storage of GM2 ganglioside and related glycolipids. We have previously found that the progressive neurologic disease induced in *Hexb*$^{-/-}$ mice, an animal model for Sandhoff disease, is associated with the production of pathogenic anti-glycolipid autoantibodies.

Methodology/Principal Findings: In our current study, we report on the alterations in the thymus during the development of mild to severe progressive neurologic disease. The thymus from *Hexb*$^{-/-}$ mice of greater than 15 weeks of age showed a marked decrease in the percentage of immature CD4^{+}/CD8^{+} T cells and a significantly increased number of CD4^{+}/CD8^{-} T cells. During involution, the levels of both apoptotic thymic cells and IgG deposits to T cells were found to have increased, whilst swollen macrophages were prominently observed, particularly in the cortex. We employed cDNA microarray analysis to monitor gene expression during the involution process and found that genes associated with the immune responses were upregulated, particularly those expressed in macrophages. CXCL13 was one of these upregulated genes and is expressed specifically in the thymus. B1 cells were also found to have increased in the thy mus. It is significant that these alterations in the thymus were reduced in *FcRγ* additionally disrupted *Hexb*$^{-/-}$ mice.

Conclusions/Significance: These results suggest that the FcRγ chain may render the usually poorly immunogenic thymus into an organ prone to autoimmune responses, including the chemotaxis of B1 cells toward CXCL13.

Citation: Kanzaki S, Yamaguchi A, Yamaguchi K, Kojima Y, Suzuki K, et al. (2010) Thymic Alterations in GM2 Gangliosidoses Model Mice. PLoS ONE 5(8): e12105. doi:10.1371/journal.pone.0012105

Editor: Joseph El Khoury, Massachusetts General Hospital and Harvard Medical School, United States of America

Received December 12, 2009; **Accepted** July 13, 2010; **Published** August 10, 2010

Funding: This work was supported by a Grant-in-Aid for Scientific Research from the Japan Society for the Promotion of Science (to SY, #17590355, 20590407 and AY, 19790734; http://www.jsps.go.jp/j-grantsinaid/) and from the Yokohama City University, Yokohama, Japan (to YN, #K200003; http://www.yokohama-cu.ac.jp/). The funders had no role in study design, data collection and analysis, decision to publish, or preparation of the manuscript.

Competing Interests: The authors have declared that no competing interests exist.

* E-mail: yamaguchiakira@mac.com

Introduction

Lysosomal storage disorders (LSDs) arise from functional defects in one or more of the proteins essential to normal lysosome function. This typically involves the enzymes that play a critical role in the intracellular digestion of glycoproteins, glycolipids, glycosaminoglycans, or other macromolecules [1]. GM2 gangliosidoses, one of the major LSDs, are caused by an abnormality in the β-hexosaminidases [1,2]. β-Hexosaminidase A consists of a heterodimer of an α-subunit (*HEXA* gene product) and a β-subunit (*HEXB* gene product) whereas β-Hexosaminidase B is a homodimer of β-subunits. Mutations in the *HEXA* gene cause Tay-Sachs disease, whereas mutations in the *HEXB* gene cause Sandhoff disease (SD) [1].

Previous studies have shown that the *Hexb*-deficient (*Hexb*$^{-/-}$) mouse develops an SD-like illness and therefore provides a useful animal model for investigating the pathophysiology of SD [3–5]. As with many of the other LSDs, neurodegeneration is a prominent feature of SD and since the neurons accumulate a large amount of GM2 ganglioside and GA2 relative to other tissues in this disease, it is generally thought that the nervous system is its main pathological target. The accumulation of GM2 ganglioside or its derivatives in the nervous system is implicated in unscheduled neuronal cell death [6]. However, recent studies have provided good evidence that GM2 ganglioside and GA2 accumulation can not account for all of the nervous system damage in *Hexb*$^{-/-}$ mice.

For example, bone marrow transplantation from normal (*Hexb*$^{+/+}$) to *Hexb*$^{-/-}$ mice suppresses neuronal death and improves survival ratios despite having no effect on either β-hexosaminidases activities or ganglioside accumulation in the brain [7–9].

We have reported in a previous study that an autoimmune response occurs in *Hexb*$^{-/-}$ mice with accompanying pathophysiological phenotypes [10]. To determine the role of anti-ganglioside autoantibodies in this earlier study, we additionally disrupted the Fc receptor gamma (*FcRγ*) gene in the *Hexb*$^{-/-}$ mouse model, as it plays a key role in immune complex-mediated autoimmune diseases. Clinical symptoms were improved and life spans were extended in the resulting double-null (*Hexb*$^{-/-}$*FcRγ*$^{-/-}$) mice, suggesting that autoantibodies play an important role in the central nervous system (CNS) pathophysiology in SD. Moreover, we found that age-matched *Hexb*$^{-/-}$*FcRγ*$^{-/-}$ mice had a reduced serum titer of anti-GA2 autoantibody when compared with *Hexb*$^{-/-}$*FcRγ*$^{+/+}$ mice, suggesting that the FcRγ dependent pathway(s) also

contribute to the production of autoantibodies [10]. Recently also, autoantibodies have been implicated in several LSDs and their respective mouse models such as MPSIIIB [11], Batten disease [12–15], and Gaucher disease [16,17]. This suggests that the production of autoantibodies is mediated by common pathway(s) among these diseases although the underlying mechanism of production remains unknown.

The thymus is a central or primary lymphoid organ responsible for the production, differentiation and direction of a population of small lymphocytes that are involved primarily with cell-mediated immunity. Such thymus-dependent lymphocytes are known as T-lymphocytes in contrast to the bone marrow dependent B-lymphocytes with which they intimately co-operate. Recently, alterations in the thymus were observed in several LSD model animals such as feline GM1 gangliosidosis [18–20], and twitcher mice [21]. In $Hexb^{-/-}$ mice, GM2 and GA2 were found to have accumulated in the thymus [22]. Impaired selection of invariant natural killer T cells was also observed in this same study [22]. However, whether such alterations in the thymus contribute to the LSD pathophysiology remains unknown.

Over the last decade, a family of chemotactic cytokines known as the chemokines has been found to be involved in the trafficking of leukocytes in both normal and pathological states. Several autoimmune diseases, such as rheumatoid arthritis, systemic lupus erythematosus, multiple sclerosis, and myasthenia gravis, are associated with inappropriate activation of the chemokine network [23]. For example, aberrant high expression of Chemokine (C-X-C motif) ligand 13 (CXCL13) in the thymus in aged (NZB × NZW) F1 (BWF1) mice may play a pivotal role in breaking immune tolerance in the thymus and in recruiting autoantibody-producing B1 cells and $CD4^+$T cells during the development of murine lupus [24–26]. B1 cells of different origin and function than conventional B cells (B2 cells) have long been considered to be involved in autoantibody production in autoimmune diseases [27–29].

In $Hexb^{-/-}$ mice, cDNA microarray analysis of the CNS has previously revealed an upregulation of inflammatory cytokines/chemokines including CXCL13, dominated by activated microglia/macrophages [8]. The expected mechanism underlying this microglia/macrophage activation was the storage of glycolipids from engulfed apoptotic neurons. Normally, most T cells are eliminated within the cortex or at the cortico-medullary junction via programmed cell death. These T cells are usually rapidly engulfed by macrophages without accompanying immune activation. It is thus possible that if the macrophages cannot degrade apoptotic T cell-derived glycolipids, they are also activated.

We hypothesize that the thymus plays an important role in the production of autoantibodies in SD. We have therefore examined the thymic alterations of $Hexb^{-/-}$ mice during the development of mild to severe progressive neurologic disease in our current study and explored the relationship between these thymic abnormalities and autoimmunity.

Results

$Hexb^{-/-}FcR\gamma^{+/+}$ mice develop progressive and age-related thymus atrophy

Our initial analysis indicated that $Hexb^{-/-}FcR\gamma^{+/+}$ mice with clinically severe neurologic signs had a severely reduced thymic mass (Fig. 1A). In comparison, age-matched $Hexb^{-/-}FcR\gamma^{-/-}$ mice had only a slight reduction in their thymic mass. To evaluate whether these thymic alterations were due to hypoplasia or premature involution, thymic tissues from younger mice were also examined quantitatively. A comparison of $Hexb^{+/-}FcR\gamma^{+/+}$, $Hexb^{-/-}FcR\gamma^{+/+}$ and $Hexb^{-/-}FcR\gamma^{-/-}$ thymic weights is shown in Figure 1B. The 15 week old $Hexb^{-/-}FcR\gamma^{+/+}$ mice showed significant (75%) loss of thymic weight when compared with age-matched $Hexb^{+/-}FcR\gamma^{+/+}$ mice. In contrast, there were no significant differences between the younger mice of both genotypes. $Hexb^{-/-}FcR\gamma^{-/-}$ mice had a slight, but statistically significant, reduction in thymic weight when compared with $Hexb^{+/-}FcR\gamma^{+/+}$ mice. Flow cytometric analysis further revealed that $CD4^+/CD8^+$ immature T cell ratio was dramatically decreased in the 15 week old $Hexb^{-/-}FcR\gamma^{+/+}$ thymus compared with that of the $Hexb^{+/-}FcR\gamma^{+/+}$ mice (5.8% vs. 88.0%), whereas the $CD4^+/CD8^-$ and $CD4^-/CD8^+$ T cell ratios were markedly increased (Fig. 1C top panel). Moreover, the $CD4^-/CD8^-$ non T cell population ratio was also increased in $Hexb^{-/-}FcR\gamma^{+/+}$ mice. In $Hexb^{-/-}FcR\gamma^{-/-}$ mice, the percentages of $CD4^+/CD8^+$, $CD4^+/CD8^-$, $CD4^-/CD8^+$, and $CD4^-/CD8^-$ cells were 87.1%, 6.8%, 3.2%, and 2.9%, respectively. The absolute number of $CD4^+/CD8^+$ T cells per thymus was severely reduced in $Hexb^{-/-}FcR\gamma^{+/+}$ mice (Fig. 1C bottom panel). In addition, the absolute number of $CD4^+/CD8^-$, $CD4^-/CD8^+$, and $CD4^-/CD8^-$ T cells per thymus was also reduced in $Hexb^{-/-}FcR\gamma^{+/+}$ mice.

Histological examination of the thymus from $Hexb^{+/-}FcR\gamma^{+/+}$, $Hexb^{-/-}FcR\gamma^{+/+}$ and $Hexb^{-/-}FcR\gamma^{-/-}$ mice

We next undertook histological analysis of the thymic tissues from $Hexb^{+/-}FcR\gamma^{+/+}$, $Hexb^{-/-}FcR\gamma^{+/+}$ and $Hexb^{-/-}FcR\gamma^{-/-}$ mice. When examined by light microscopy, the histological findings from younger $Hexb^{-/-}FcR\gamma^{+/+}$ mice were found not to significantly differ from $Hexb^{+/-}FcR\gamma^{+/+}$ mice. In the 15 week old $Hexb^{-/-}FcR\gamma^{+/+}$ mice, the cellular density did not appear to be altered in the medulla of the thymus but the cortices or cortico-medullary junctions were frequently indistinct (Fig. 2). Moreover, many foamy macrophages could be observed not only in the medullary area, but also the cortex area in these mice. Some macrophages were also found to contain hematoxylin-positive nuclear particles in their cytoplasm. Cortices or cortico-medullary junctions were clearly detectable in the thymus of $Hexb^{-/-}FcR\gamma^{-/-}$ mice and foamy macrophages were also present in $Hexb^{-/-}FcR\gamma^{-/-}$mice. We also examined the immunofluorescent analysis of GA2 and thymocyte, for each thymus derived from $Hexb^{+/-}FcR\gamma^{+/+}$, $Hexb^{-/-}FcR\gamma^{+/+}$ and $Hexb^{-/-}FcR\gamma^{-/-}$ mice. In the 15 week old $Hexb^{+/-}FcR\gamma^{+/+}$ mice, GA2 was stained on the cell membrane of CD4 and/or CD8 positive T cells (Fig. S1). Age matched $Hexb^{-/-}FcR\gamma^{+/+}$ mice showed the marked decrease of the T cells in the cortex area. In contrast, GA2 was stained in those areas, and it seems to be accumulating in the cytosol of the foamy cells. The decrease of the T cell and the accumulation of GA2 were not more clearly observed in the presymptomatic stage of $Hexb^{-/-}FcR\gamma^{+/+}$, and $Hexb^{-/-}FcR\gamma^{-/-}$ mice. These results suggest the possibility that the localization of GA2 was moved from T cells to foamy macrophages during the involution.

Histological examination of a thymus from a human SD patient

To determine whether thymic alterations can also be detected in a human case of SD, we obtained a H&E stained tissue sample from an SD patient for examination. The histology of this thymic sample revealed that the cortical cells were severely reduced and that the cortico-medullary junctions could not be clearly observed (Fig. 3). Furthermore, most of the cortical and medullary cells harbored a vacuolated cytoplasm.

Increased cell death in the thymus of 15 week old $Hexb^{-/-}FcR\gamma^{+/+}$ mice

The thymic tissues from 15 week old $Hexb^{+/-}FcR\gamma^{+/+}$ and $Hexb^{-/-}FcR\gamma^{+/+}$ mice were further analyzed by transmission

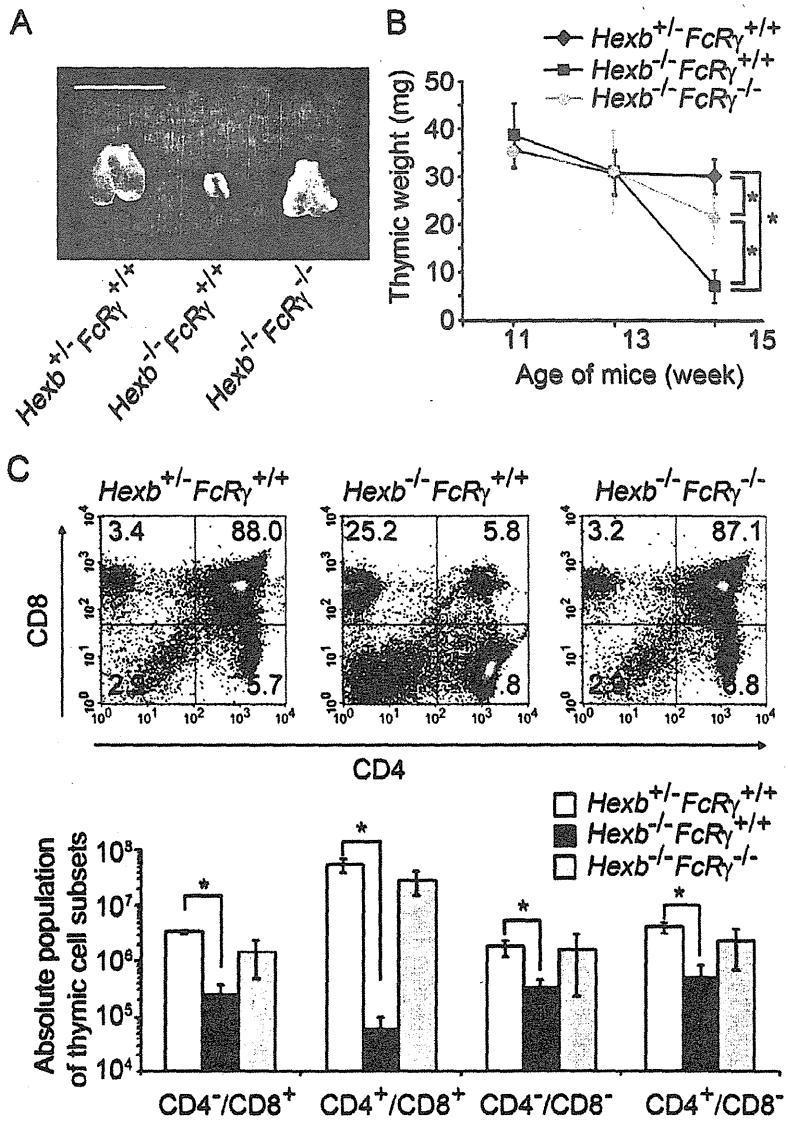

Figure 1. ***Hexb*$^{-/-}$*FcRγ*$^{+/+}$ **mice show progressive, age-related thymus atrophy.** (A) The thymus was removed from 15 week old *Hexb*$^{+/-}$*FcRγ*$^{+/+}$, *Hexb*$^{-/-}$*FcRγ*$^{+/+}$ and *Hexb*$^{-/-}$*FcRγ*$^{-/-}$ mice. Scale bar, 1 cm. (B) Thymic tissues from *Hexb*$^{+/-}$*FcRγ*$^{+/+}$, *Hexb*$^{-/-}$*FcR*$^{+/+}$ and *Hexb*$^{-/-}$*FcR*$^{-/-}$ mice at 11, 13 and 15 weeks of age were removed and weighed. The data shown are expressed as the mean (S.D. of 3–14 mice for each group per time point. *$P<0.01$. (C) Thymic cells from *Hexb*$^{+/-}$*FcR*$^{+/+}$, *Hexb*$^{-/-}$*FcR*$^{+/+}$ and *Hexb*$^{-/-}$*FcR*$^{-/-}$ mice were stained with CD4 and CD8 antibodies. The percentages of T cell subsets were then determined by flow cytometry. The profiles for each genotype are indicated in the top panels. The absolute cell numbers for each subpopulation of the thymus were calculated from the total number of thymic cells (mean (S.D.; $n=3$–4). *$P<0.05$.
doi:10.1371/journal.pone.0012105.g001

electron microscopy (TEM). In the *Hexb*$^{-/-}$*FcRγ*$^{+/+}$ mice, the macrophages contained numerous abnormal nuclear-like electron dense particles, which were not evident in the *Hexb*$^{+/-}$*FcRγ*$^{+/+}$ thymus (Fig. 4A). These macrophages were also found to contain many vacuoles with characteristics of lysosomal storage vessels. To better understand the progressive reduction observed in the number of thymic cells, we analyzed thymic cell death using a TUNEL assay. TUNEL-positive cells were more frequently found in the *Hexb*$^{-/-}$*FcRγ*$^{+/+}$ cortex and medulla than in the corresponding regions of the *Hexb*$^{+/-}$*FcRγ*$^{+/+}$ thymus (Fig. 4B). TUNEL-positive particles could be seen inside the macrophages, and were thought to correspond to the nuclear-like particles observed by TEM. We next quantified the number of apoptotic and necrotic cells by flow cytometry. The results showed that the numbers of AnnexinV^{+}/PI^{-} apoptotic cells in *Hexb*$^{+/-}$*FcRγ*$^{+/+}$, *Hexb*$^{-/-}$*FcR*$^{+/+}$ and *Hexb*$^{-/-}$*FcR*$^{-/-}$ mice were 1.28±0.44, 7.06±2.32, and 1.79±0.45 respectively. Moreover, AnnexinV+/PI+ late apoptotic/necrotic cells were found to have increased in the *Hexb*$^{-/-}$*FcR*$^{+/+}$ thymus (1.47±0.68, 6.45±1.87, and 1.85±0.69, respectively; Fig. 4C). Since thymic cell death in the *Hexb*$^{-/-}$*FcR*$^{-/-}$ mice is decreased, we hypothesized that the immune-complex mediated response is responsible for accelerating thymic cell death in *Hexb*$^{-/-}$*FcR*$^{+/+}$ mice. Indeed, we found a marked increase in the percentage of IgG/TCR-(double positive T cells (0.53±0.20% vs. 1.96±0.67%), suggesting that IgG is bound to the T cell membrane, in the 15 week old *Hexb*$^{-/-}$*FcR*$^{+/+}$ mice as compared with age-matched *Hexb*$^{+/-}$*FcR*$^{+/+}$ mice. The 15 week old

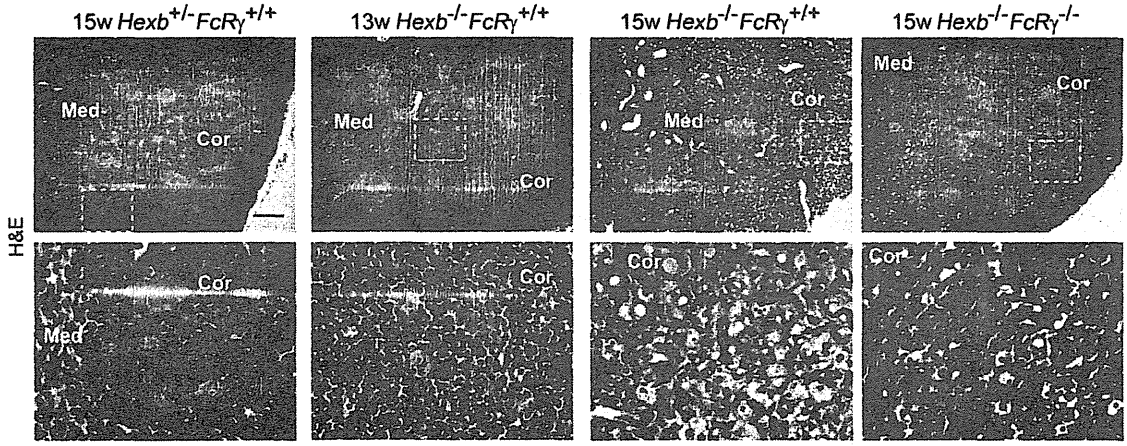

Figure 2. Histological examination of the thymus from *Hexb*$^{+/-}$*FcRγ*$^{+/+}$, *Hexb*$^{-/-}$*FcRγ*$^{+/+}$ and *Hexb*$^{-/-}$*FcRγ*$^{-/-}$ mice. H&E staining of paraffin-embedded thymic sections from 13 week old *Hexb*$^{+/-}$*FcRγ*$^{+/+}$, 15 week old *Hexb*$^{+/-}$*FcRγ*$^{+/+}$, *Hexb*$^{-/-}$*FcRγ*$^{+/+}$ and *Hexb*$^{-/-}$*FcRγ*$^{-/-}$ mice. The bottom panels show a higher magnification image of the framed area in the top panels. Cor, cortex; Med, medulla. Arrows indicate vacuolated cells. Scale bars, top panel, 100 μm; bottom panel, 50 μm.
doi:10.1371/journal.pone.0012105.g002

Hexb$^{-/-}$*FcR*$^{-/-}$ mice also showed a reduction in this population of cells (Fig. 4D).

Macrophage activation and expansion in thymus

The swelling of macrophages is a prominent feature of many LSDs. To confirm whether the swollen cells we observed by H&E staining of our thymic sections were macrophages, we stained these samples with Iba-1 and found that positive cells were rarely observed in the cortices of the 15 week old *Hexb*$^{+/-}$*FcR*$^{+/+}$ mice. 13 week old *Hexb*$^{-/-}$*FcR*$^{+/+}$ mice were found not to significantly differ from *Hexb*$^{+/-}$*FcRγ*$^{+/+}$ mice. On the other hand, numerous Iba-1 positive swelling cells were detected in the 15 week old *Hexb*$^{-/-}$*FcR*$^{+/+}$ thymus, particularly in the cortex. In *Hexb*$^{-/-}$*FcR*$^{-/-}$ mice, at 15 weeks of age, the numbers of both foamy cells and amoeboid, Iba-1-positive thymic macrophages were substantially reduced compared with the *Hexb*$^{-/-}$*FcR*$^{+/+}$ mice (Fig. 5A). To determine whether the percentage of macrophages among the total thymic cell population was increased, we performed flow cytometric analysis. The percentage of thymic macrophages from 15 week old *Hexb*$^{+/-}$*FcR*$^{+/+}$, *Hexb*$^{-/-}$*FcR*$^{+/+}$ and *Hexb*$^{-/-}$*FcR*$^{-/-}$ mice was 0.93±0.38, 4.36±0.66 and 1.48±0.25% respectively (Fig. 5B). Recent studies have reported that the up-regulation of the Mip-1α correlates with monocyte infiltration and the pathogenesis of SD [30]. To quantify the increase in Mip-1α mRNA in the thymus of 15 week old *Hexb*$^{-/-}$*FcRγ*$^{+/+}$ mice, the gene expression ratios of Mip-1α relative to ribosomal protein s18 were measured by real-time RT-PCR. A 24.6-fold increase in Mip-1α expression was detected in the thymus of *Hexb*$^{-/-}$*FcRγ*$^{+/+}$ mice in comparison with *Hexb*$^{+/-}$*FcRγ*$^{+/+}$ mice. In addition, *Hexb*$^{-/-}$*FcRγ*$^{-/-}$ mice showed a 2.69-fold higher expression of Mip-1α mRNA compared with the *Hexb*$^{+/-}$*FcRγ*$^{+/+}$ mice (Fig. 5C).

mRNA expression profile in the thymus of *Hexb*$^{-/-}$*FcRγ*$^{+/+}$ mouse

To further elucidate the molecular basis of thymic involution, we performed cDNA microarray analysis to identify the changes in gene expression that accompanied the involution of the thymus. Thymic gene expression of 15 week old *Hexb*$^{+/-}$*FcRγ*$^{+/+}$ and *Hexb*$^{-/-}$*FcRγ*$^{+/+}$ mice were examined with Affymetrix® Mouse Genome 430 2.0 Array containing 45101unique mouse gene sequences. The gene expression profile reported in this paper has been deposited in the Gene Expression Omnibus (GEO) database (http://www.ncbi.nlm.nih.gov/geo: accession no. GSE19641). 8018 probes were found to be relatively increased in the thymus of the *Hexb*$^{-/-}$*FcRγ*$^{+/+}$ mice compared with that of the *Hexb*$^{+/-}$*FcRγ*$^{+/+}$ mice. On the other hand, the expression of 7604 probes was relatively decreased. The cohort of up-regulated sequences was dominated by genes that play a role in the immune response. In addition, some of these genes are expressed in macrophage

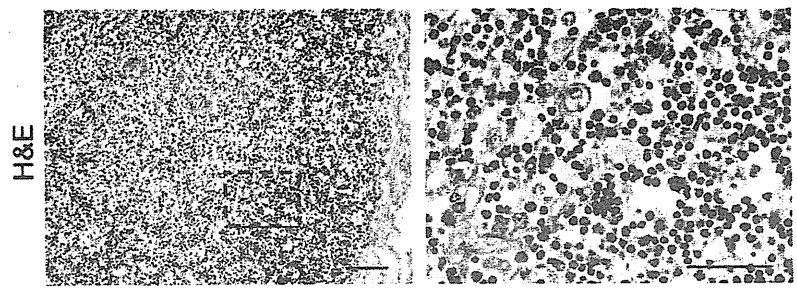

Figure 3. Histological examination of a thymus from an SD patient. H&E staining of a paraffin-embedded thymic section from an 11 month-old SD patient. The right panel shows a higher magnification of the framed area in the left panel. Scale bars, left panel, 100 μm; right panel, 50 μm.
doi:10.1371/journal.pone.0012105.g003

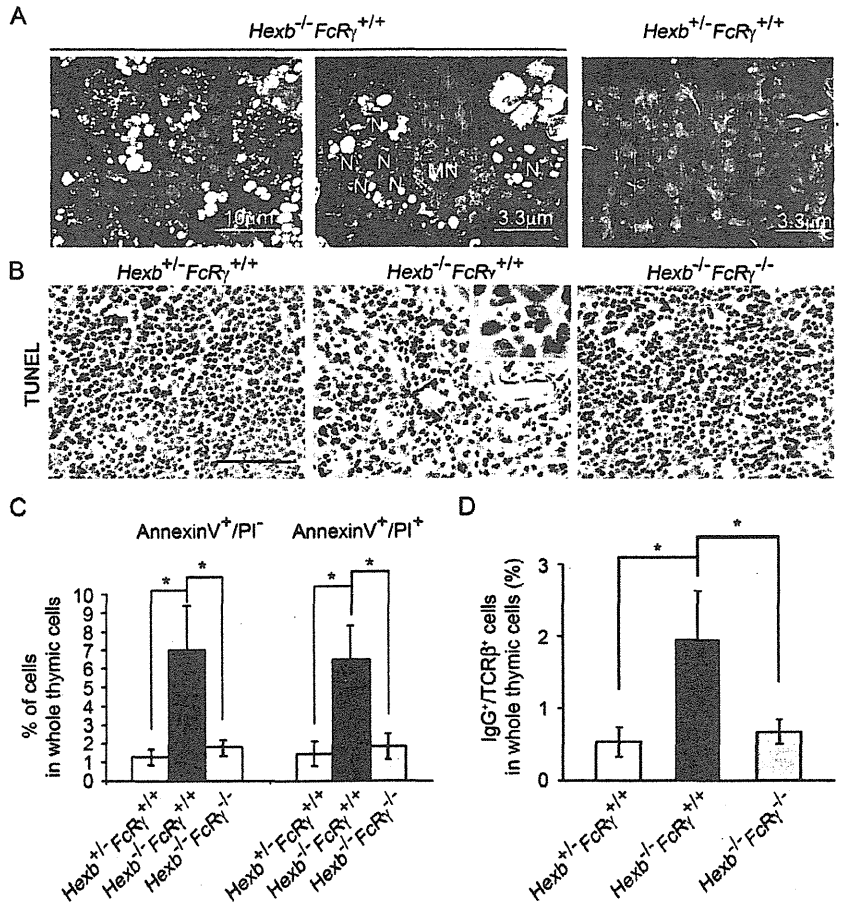

Figure 4. Increased cell death in the thymus of the 15 week old *Hexb*$^{-/-}$*FcRγ*$^{+/+}$ mouse. (A) Thymic sections from 15 week old *Hexb*$^{-/-}$*FcRγ*$^{+/+}$ and *Hexb*$^{+/-}$*FcRγ*$^{+/+}$ mice were analyzed by TEM. Left panel, at lower magnification many electron dense materials and vacuoles are evident. Middle panel, nucleus-like electron dense particles and vacuoles are visible in the cytoplasm of the macrophages at higher magnification. Right panel, nuclear particles were not confirmed in the thymus of the *Hexb*$^{+/-}$*FcRγ*$^{+/+}$ mouse.N, nucleus particle-like structure; MN, macrophage nucleus. (B) Paraffin-embedded thymic sections from *Hexb*$^{+/-}$*FcRγ*$^{+/+}$, *Hexb*$^{-/-}$*FcRγ*$^{+/+}$ and *Hexb*$^{-/-}$*FcRγ*$^{-/-}$ mice were stained using the TUNEL method. Scale bar, 50((m. A higher magnification image of the arrow position in the middle panel is shown in the right shoulder frame. (C) Thymic cells from *Hexb*$^{+/-}$*FcR*$^{+/+}$, *Hexb*$^{-/-}$*FcR*$^{+/+}$ and *Hexb*$^{-/-}$*FcR*$^{-/-}$ mice were stained with FITC conjugated anti-Annexin V antibody and PI, and the percentages of dying cells were determined by flow cytometry ($n = 4$–8). *P<0.01. (D) IgG deposition in TCR(-positive T cells analyzed by flow cytometry ($n = 3$–5). *$P \leq 0.01$.
doi:10.1371/journal.pone.0012105.g004

lineages such as macrophage expressed gene 1, and colony stimulating factor 2 receptor beta 1. Th2 cytokines were mostly upregulated in the *Hexb*$^{-/-}$*FcRγ*$^{+/+}$ mice, although Th1 cytokines did not show this increase (Table 1). In addition, B cell-related genes such as CD19, CXCL13 were increased, whereas the T cell-related genes were mostly decreased, in *Hexb*$^{-/-}$*FcRγ*$^{+/+}$ mice compared with *Hexb*$^{+/-}$*FcRγ*$^{+/+}$ mice.

Marked increase in CXCL13 expression in the thymus of the *Hexb*$^{-/-}$*FcRγ*$^{+/+}$ mouse

Quantitative differences in CXCL13 expression in the thymus between *Hexb*$^{+/-}$*FcRγ*$^{+/+}$, *Hexb*$^{-/-}$*FcRγ*$^{+/+}$ and *Hexb*$^{-/-}$*FcRγ*$^{-/-}$ mice were assayed by real-time RT-PCR (Fig. 6A). There were no significant differences found in 11 or 13 week old *Hexb*$^{+/-}$*FcRγ*$^{+/+}$, *Hexb*$^{-/-}$*FcRγ*$^{+/+}$ and *Hexb*$^{-/-}$*FcRγ*$^{-/-}$ mice. However, an extremely high level of CXCL13 expression was observed in the thymus of 15 week old *Hexb*$^{-/-}$*FcRγ*$^{+/+}$ mice compared with the normalized CXCL13 levels in *Hexb*$^{+/-}$*FcRγ*$^{+/+}$ (23.3-fold) and *Hexb*$^{-/-}$*FcRγ*$^{-/-}$ mice. The expression of several other cytokines/chemokines such as SDF-1 and TNF-α was not increased in *Hexb*$^{-/-}$*FcRγ*$^{+/+}$ mice compared with *Hexb*$^{+/-}$*FcRγ*$^{+/+}$ mice (data not shown). To assess whether the abnormal CXCL13 mRNA expression is thymus-specific, we quantified the CXCL13 mRNA levels in other lymphoid organs. The upregulation of CXCL13 was not found in the lymph nodes or spleen (Fig. 6B). In the thymus of 15week old *Hexb*$^{-/-}$*FcRγ*$^{+/+}$ mice, the normal architecture was lost and CXCL13 was diffusely distributed throughout the entire region (Fig. 6C). Real-time RT-PCR analysis of magnetic cell sorted leukocyte subpopulations demonstrated that CXCL13 is highly expressed in thymic CD11b-positive cells, which are putatively regarded as macrophages, and also in dendritic cells obtained from 15 week old *Hexb*$^{-/-}$*FcRγ*$^{+/+}$ mice, but not in CD11b-negative cells from these animals (Fig. 6D).

The B1 and B2 cell populations are markedly increased in the thymus of *Hexb*$^{-/-}$*FcRγ*$^{+/+}$ mouse

The aberrantly high expression of CXCL13 in the thymus of mice with murine lupus plays a pivotal role in recruiting

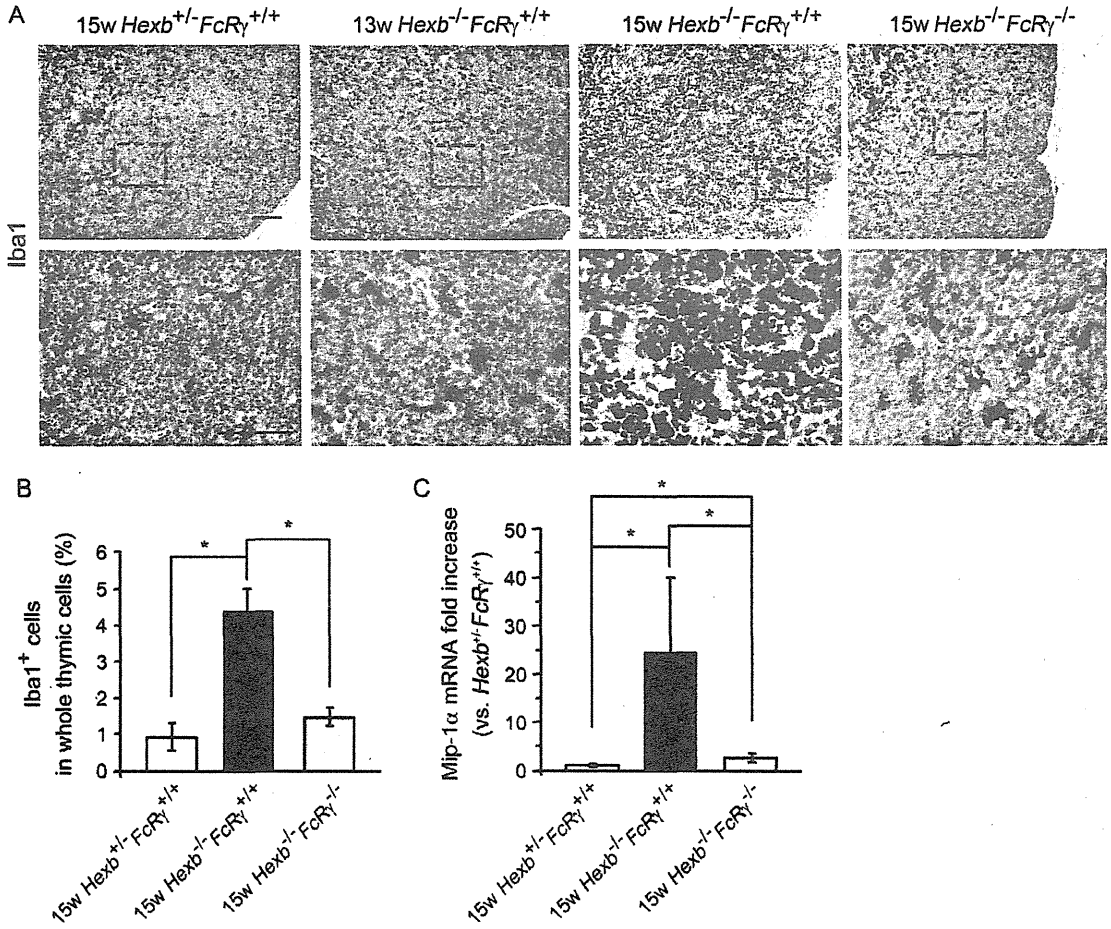

Figure 5. Macrophage activation and expansion. (A) Thymic tissues from 13 week old $Hexb^{+/-}FcR^{+/+}$, 15 week old $Hexb^{+/-}FcR^{+/+}$, $Hexb^{-/-}FcR^{+/+}$ and $Hexb^{+/-}FcR^{+/+}$ mice were stained with antibodies against the macrophage marker Iba1 and processed using the avidin-biotin-peroxidase complex (ABC) method. The bottom panels show higher magnifications of the framed areas in the top panels. Scale bars, top panel, 100(μm; bottom panel, 50 μm. (B) Thymic cells from15 week old $Hexb^{+/-}FcR\gamma^{+/+}$, $Hexb^{-/-}FcR\gamma^{+/+}$ and $Hexb^{-/-}FcR\gamma^{-/-}$ mice were stained with anti-Iba1 followed by Alexa Fluor 488® conjugated anti-rabbit IgG (H+L), and the percentages of macrophages were determined by flow cytometry ($n=4$). *$p<0.01$. (C) Mip-1α mRNA levels in the thymus from 15week old $Hexb^{-/-}FcR\gamma^{+/+}$ and $Hexb^{-/-}FcR\gamma^{-/-}$ mice were assayed by Real-time RT-PCR and these values were compared with those of the $Hexb^{+/-}FcR\gamma^{+/+}$ mouse (mean ± S.D.; $n=5$–9). *$P<0.05$.
doi:10.1371/journal.pone.0012105.g005

autoantibody-producing B cells. We evaluated whether B cells are increased also in the thymus of 15 week old $Hexb^{-/-}FcR\gamma^{+/+}$ mice. By histological examination, we detected massive CD19-positive B cell infiltration and/or expansion in the thymus of the 15 week old $Hexb^{-/-}FcR\gamma^{+/+}$ mice (Fig. 7A). In 13 week old $Hexb^{-/-}FcR\gamma^{+/+}$ and 15 week old $Hexb^{-/-}FcR\gamma^{-/-}$ mice, we did not see this B cell expansion. The percentages of $CD19^+/CD5^+/B220^{lo}$ B1 cells were 0.12±0.04, 0.68±0.28 and 0.23±0.07% in the thymus of 15 week old $Hexb^{+/-}FcR\gamma^{+/+}$, $Hexb^{-/-}FcR\gamma^{+/+}$ and $Hexb^{-/-}FcR\gamma^{-/-}$ mice, respectively, and those of $CD19^+/CD5^-/B220^{hi}$ B2 cells were 0.11±0.05, 0.53±0.19 and 0.17±0.06% respectively (Fig. 7B).

Discussion

Sandhoff disease is a lysosomal storage disorder characterized by the absence of β-hexosaminidase and storage of GM2 ganglioside and related glycolipids. It is widely postulated that the CNS is the main pathological target of GM2 gangliosidosis. However, we have previously found that the production of autoantibodies plays an important role in the pathogenesis of neuropathy in Sandhoff disease [10]. In our present study, we observed a dramatic involution of the thymus in 15 week old $Hexb^{-/-}FcR\gamma^{+/+}$ mouse. The thymus plays a crucial role in immune system homeostasis, and thymic abnormalities have been previously reported in many autoimmune diseases, such as myasthenia gravis [31], systemic sclerosis [32], in a mouse model of systemic lupus erythematosus [24], and multiple sclerosis [33]. Since autoimmunity is found also in SD, the contribution of thymus abnormalities to the pathogenesis of this disease seems plausible. We therefore tested for immunological alterations in the thymus of $Hexb^{-/-}FcR^{+/+}$ mice during the development of mild to severe progressive neurologic disease and explored the relationship between thymic abnormalities and autoimmunity.

The thymus of the $Hexb^{-/-}FcR^{+/+}$ mouse was found to be drastically involuted at the late stages, whereas this degree of involution was reduced in the $Hexb^{-/-}FcR\gamma^{-/-}$ mouse (Fig. 1A, B), suggesting that this process is dependent on the FcR(chain. The involution itself was found to contain a markedly decreased

Table 1. mRNA expression profile in the thymus of the 15 week old *Hexb*$^{-/-}$*FcRγ*$^{+/+}$ mouse.

Gene name (*Symbol*)	Base signal	Exp signal	Exp/Base signal Log ratio
T lymphocyte			
CD3 antigen, delta (*Cd3d*)	4510.3	1509.6	−1.6
CD4 antigen (*Cd4*)	1438.6	378.3	−1.8
CD8 antigen, alpha chain (Cd8a)	5002.2	235.3	−4.3
T-cell receptor alpha chain (*Tcra*)	55.1	15.1	−2.1
Macrophage			
Colony stimulating factor 2 receptor, beta 1 (*Csfr2b1*)	143	549.9	2.1
Macrophage ecpressed gene 1 (*Mpeg1*)	836.4	1905.2	1.3
Macrophage migration inhibitory factor (*Mif*)	2844.4	1810	−0.6
Monocyte to macrophage differentiation-asociated (*Mmd*)	328.9	592.2	0.8
B lymphocyte			
Early B-cell factor 1 (*Ebf1*)	17.9	144.5	3.1
CD79A antigen (*Cd79a*)	65.7	227.2	1.6
CD79B antigen (*Cd79b*)	155.7	407.5	1.4
CD19 antigen (*Cd19*)	6.7	125.3	3.8
CD38 antigen (*Cd38*)	167.5	497.9	1.9
Burkitt lymphoma receptor 1 (*Cxcr5*)	15.6	80.3	2.6
Chemokine			
Chemokine (C-X-C motif) ligand 13 (*Cxcl13*)	29	677.1	4.6
Th2 cytokine			
Interleukin 10 (*Il10*)	3.6	24.3	2.2
Interleukin 10 receptor, alpha (*Il10ra*)	49.2	118.4	1.2
Interleukin 10 receptor, beta (*Il10rb*)	330.8	742.2	1.3
Interleukin 13 receptor, alpha 1 (*Il13ra1*)	58.3	128.9	1.1
Th1 cytokine			
Tumor necrosis factor (*Tnf*)	14.1	50.4	1.9
Transforming growth factor, beta 1 (*Tgfb1*)	455	213	−0.9

The Affymetrix® Mouse Genome 430 2.0 Array was employed to identify changes in the gene expression profile in the thymus of a 15 week old of *Hexb*$^{-/-}$*FcRγ*$^{+/+}$ mouse. 'Signal' represents a measure of the relative abundance of a particular transcript. 'Exp/Base signal Log ratio' denotes the change in the expression level for a transcript between Base group (15 week old *Hexb*$^{+/-}$*FcRγ*$^{+/+}$ thymus) and the Experimental group (15 week old *Hexb*$^{-/-}$*FcRγ*$^{+/+}$ thymus). This change is expressed as the log2 ratio. A log2 ratio of 1 is equivalent to a fold Change of 2. Representative genes that function in the immune system are listed.
doi:10.1371/journal.pone.0012105.t001

percentage of immature CD4+/CD8+ T cells and significantly increased populations of CD4+/CD8- cells, CD4-/CD8+ T cells and CD4-/CD8- cells (Fig. 1C, top panel). The absolute number of each subpopulation was decreased, suggesting that the changes in cell number are strongly dependent on the decreased number of CD4+/CD8+ T cells, rather than the increase in CD4+/CD8- cells, CD4-/CD8+ T cells and CD4-/CD8- cells. In contrast, no differences could be clearly observed in the younger *Hexb*$^{-/-}$ *FcR*$^{+/+}$ mice. Zhou and co-workers have also shown in their previous study that the development of classical, naive, and memory CD4 and CD8 T cells is unaffected by a *Hexb* deficiency [34]. The authors did not however discuss the state of the thymus in later stages. In other LSDs, alterations in the last stage thymus have been previously reported in feline GM1 gangliosidosis [19,20]. Flow cytometric analyses showed a marked decrease in the percentage of immature CD4$^+$/CD8$^+$ T cells and a significant increase in CD4$^-$/CD8$^+$ cells in GM1 mutant cats of greater than 210 days of age when compared with normal age matched cats [19]. Thymic involution has also been described in twitcher mice [21] and may therefore be a common pathological state among the LSDs.

We next examined for histological abnormalities in the thymus of *Hexb*$^{-/-}$*FcRγ*$^{+/+}$ mice. In the 15 week old animals, the cellular density of the thymic cortices was found to be severely reduced as a result of a decreased number of CD4$^+$/CD8$^+$ cells (Fig. 2). However, numerous macrophages with a "foamy" appearance were found instead in this region. Some of these macrophages contained hematoxylin-positive particles in their cytoplasm, suggesting that the population of apoptotic thymic cells was rapidly increased and/or that the macrophages had a diminished phagocytic capacity. Importantly, a pathology similar to that evident in mouse models appears to exist also in human SD (Fig. 3). Moreover, atrophy of the thymus has previously been described in an autopsy case report by Takahashi *et al.* [35], and in a personal communication from Tatematsu *et al.* [36]. These observations suggest that thymic alterations occur in SD in both mouse and human via a common mechanism.

We next found in our mouse model that during thymic involution, nuclear particles in the cytoplasm of the macrophages, apoptotic thymic cells, and IgG deposition to the thymic cells were all increased, particularly in the cortex (Fig. 4). Most thymic lymphocytes are cleared by normal apoptotic processes but

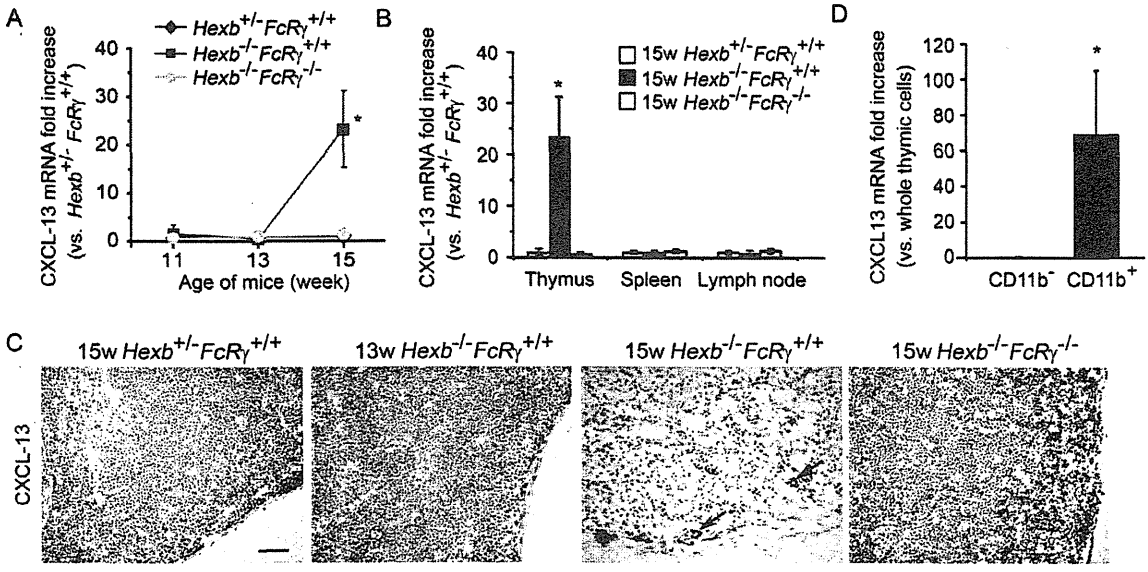

Figure 6. CXCL13 expression is markedly increased in the thymus of the 15 week old *Hexb*$^{-/-}$*FcRγ*$^{+/+}$ mouse. (A) The CXCL13 mRNA levels in the thymus from each of the *Hexb*$^{+/-}$*FcRγ*$^{+/+}$, *Hexb*$^{-/-}$*FcRγ*$^{+/+}$ and *Hexb*$^{-/-}$*FcRγ*$^{-/-}$ mice at 11, 13 and 15 weeks of age were determined by real-time RT-PCR and compared with the levels in the *Hexb*$^{+/-}$*FcRγ*$^{+/+}$ mouse (mean ± S.D.;$n=3$–8). *$P<0.05$. (B) The CXCL13 mRNA levels in the thymus, spleen and lymph nodes from 15 weeks old *Hexb*$^{+/-}$*FcRγ*$^{+/+}$, *Hexb*$^{-/-}$*FcRγ*$^{+/+}$ and *Hexb*$^{-/-}$*FcRγ*$^{-/-}$ mice was also measured using real-time RT-PCR and compared with the levels in *Hexb*$^{+/-}$*FcRγ*$^{+/+}$ mice (mean ± S.D.; $n=4$–8). *$P<0.05$. (C) Thymus cryosections from 13 week old *Hexb*$^{+/-}$*FcRγ*$^{+/+}$, 15 week old *Hexb*$^{+/-}$*FcRγ*$^{+/+}$, *Hexb*$^{-/-}$*FcRγ*$^{+/+}$ and *Hexb*$^{-/-}$*FcRγ*$^{-/-}$ mice were stained with CXCL13 antibodies and detected using DAB. Arrows indicate CXCL13-positive cells. Scale bar, 50 μm. (D) Thymic cells from 15 week old *Hexb*$^{-/-}$*FcRγ*$^{+/+}$ mice were cell sorted using MACS. The CXCL13 mRNA levels in the CD11b^{+} and CD11b^{-} cell populations are expressed relative to the normalized CXCL13 levels in whole thymic cells (mean ± S.D.; $n=4$). *$P<0.05$.
doi:10.1371/journal.pone.0012105.g006

increased apoptosis can be observed in some animal models of LSD such as twitcher mice, and feline GM1 gangliosidosis. It is thought that the accumulation of GM2 induces neuronal cell death in GM2 gangliosidosis. Various extra-neural organs also contain many minor ganglioside components. In particular, the thymus has been found to have a very complex and characteristic spectrum of ganglioside species [37,38]. Gadola et al have previously observed that glycolipids are stored in the thymus [22]. In addition, Zhou *et al.* have reported that GM1, GM2, GM3, and GT1b can induce apoptosis in thymocytes in vitro [18]. We have also confirmed in our experiments that GM2 enhances thymic cell death, resulting in the formation of *in vivo*-like T cell subpopulations *in vitro* (data not shown). However, we also found that the apoptosis and necrosis of thymic cells is decreased in 15 week old *Hexb*$^{-/-}$*FcRγ*$^{-/-}$ mice, although the accumulation levels did not obviously differ from *Hexb*$^{-/-}$*FcRγ*$^{+/+}$ mice (data not shown). This result suggests that the Fc receptor plays a role in thymic cell death in *Hexb*$^{-/-}$*FcRγ*$^{+/+}$ mice. We have previously detected the presence of anti-GM2 and anti-GA2 autoantibodies in end stage *Hexb*$^{-/-}$*FcRγ*$^{+/+}$ mice [10] and also other autoantibodies such as anti-ssDNA (unpublished data), which suggests the presence of polyclonal antibodies in *Hexb*$^{-/-}$*FcRγ*$^{+/+}$ mice. In our present study, we observed the deposition of IgG on T cell membranes (Fig. 4E). These findings suggest that an anti-T cell autoantibody is produced during the last stages in *Hexb*$^{-/-}$*FcRγ*$^{+/+}$ mice and that an IgG-FcR mediated pathway plays a role in the thymic involution seen in *Hexb*$^{-/-}$*FcRγ*$^{+/+}$ mice.The thymus from *Hexb*$^{-/-}$*FcRγ*$^{+/+}$ mice older than 15 weeks showed a marked increase in the percentage of macrophages, particularly in the cortex (Fig. 5A, B). Additionally, these macrophages were found to contain many nuclear particles in the cytoplasm. These results are consistent with the findings of previous histological experiments using H&E, TEM and TUNEL analyses. Mip-1α which is an important molecule in the pathogenesis of *Hexb*$^{-/-}$ mice [39], is upregulated in the thymus of 15 week old *Hexb*$^{-/-}$*FcRγ*$^{+/+}$ mice. The evidence suggests therefore that the increase in the number of macrophages is partly due events that occur peripherally to the thymus.

To better understand the molecular basis of thymic involution, we performed cDNA microarray analysis to identify the changes in gene expression that accompanied involution in this gland. The results revealed an upregulation of immune response associated genes dominated by macrophages. A question that then emerged was how the macrophages were activated at this stage. It is very possible that enhanced cell death and/or the FcRγ dependent signaling pathway is involved in the mechanism. Further analysis is needed to determine whether the FcRγ pathway does contribute to gene expression changes in the thymus. On the other hand, prior to autoantibody production, FcRγ independent pathways may induce thymic alterations. In this regard, previous reports have indicated that in the CNS of *Hexb*$^{-/-}$ mice, the accumulation of undegraded glycolipids in glial cells might be a trigger of pro-inflammatory cytokine/chemokine production [8,40]. It has also been reported that the induction of Mip-1α might coincide with the accumulation of *N*-acetylhexosaminyl glycoconjugates due to a *Hexb* deficiency in glial cells [31]. It is also known that macrophages accumulate considerable levels of glycolipids within late endosomes/lysosomes during the onset of Sandhoff disease [22].

We detected many vacuoles in the cytoplasm of thymic macrophages, which we speculated to be lysosomal storage (Fig. 4A). Moreover, Periodic acid-Schiff (PAS) positive glycocon-

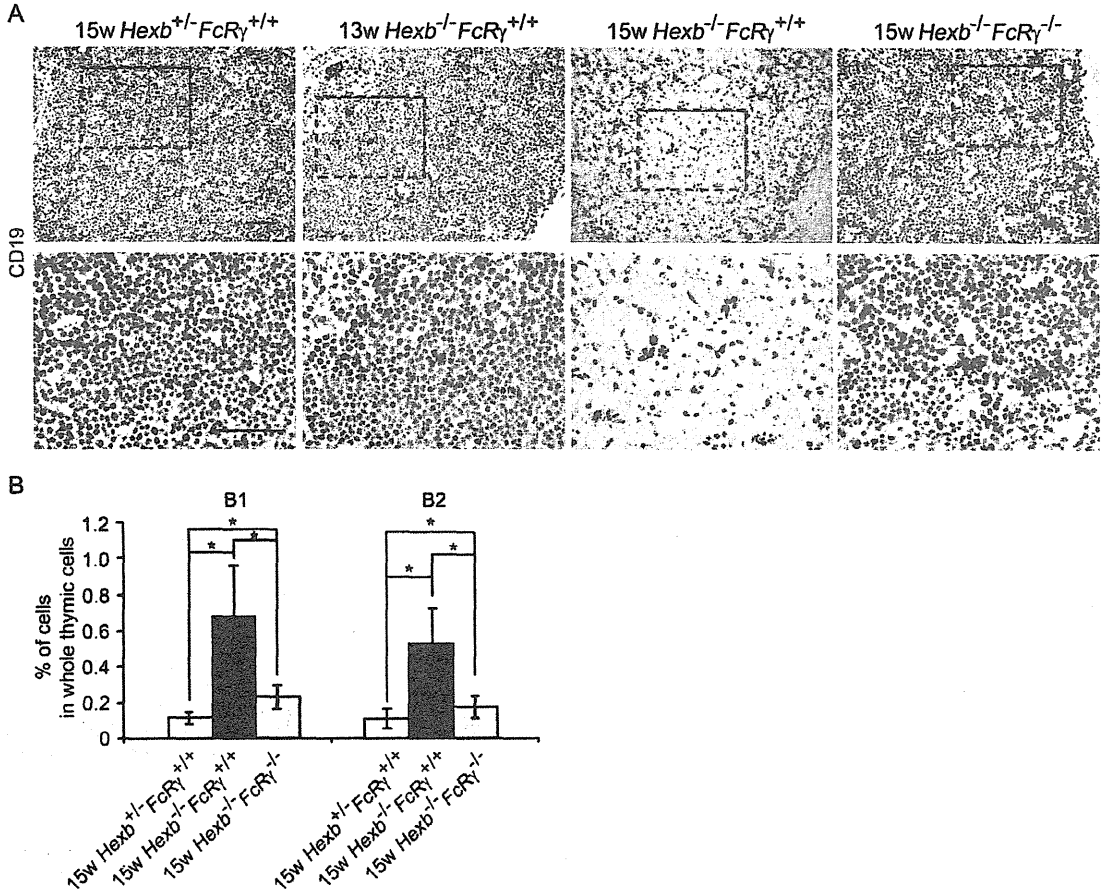

Figure 7. Significant increase in the B1 and B2 cell number in the thymus of 15 week old *Hexb*$^{-/-}$*FcRγ*$^{+/+}$ mouse. (A) Thymus cryosections from 13 week old *Hexb*$^{+/-}$*FcRγ*$^{+/+}$, 15 week old *Hexb*$^{+/-}$*FcRγ*$^{+/+}$, *Hexb*$^{-/-}$*FcRγ*$^{+/+}$ and *Hexb*$^{-/-}$*FcRγ*$^{-/-}$ mice were stained with CD19 monoclonal antibodies and detected using the ABC method. The bottom panels show higher magnification images of the framed areas in the top panels. Scale bars, 50 μm. (B) Thymic cells from 15 week old *Hexb*$^{+/-}$*FcRγ*$^{+/+}$, *Hexb*$^{-/-}$*FcRγ*$^{+/+}$ and *Hexb*$^{-/-}$*FcRγ*$^{-/-}$ mice were stained with FITC-CD5, PE-B220 and PE-Cy5-CD19 antibodies and the percentages of the B cell subsets were determined by flow cytometry (mean ± S.D.; $n = 6$–9). *$P<0.01$.
doi:10.1371/journal.pone.0012105.g007

jugates were found to accumulate in the cytoplasm of thymic macrophages (data not shown). Previously, Kawane *et al.* found that DNaseII-deficient mice developed a rheumatoid arthritis-like disease [41] and concluded that, if macrophages cannot degrade mammalian DNA from erythroid precursors and apoptotic cells, they produce TNF-α, which activates synovial cells to produce various cytokines, leading to the development of chronic polyarthritis. DNaseII-deficient mice and *Hexb*$^{-/-}$*FcRγ*$^{+/+}$ mice have a common phenotype in which undegraded substances accumulate in the macrophages. It has been postulated that a Toll-like receptor independent pathway underlies the molecular mechanism by which cells sense the DNA that has escaped from degradation and initiate an autoimmune response. Other recent reports suggest also that the NALP3 inflammasome senses lysosomal damage as an endogenous 'danger' signal and thus induces inflammation in many diseases [42–46]. The accumulation of glycolipids within macrophages, and also following the activation of the inflammasome, may therefore be related to the gene expression changes we observe in the thymus of *Hexb*$^{-/-}$*FcRγ*$^{+/+}$ mice.

CXCL13, an upregulated gene in end stage *Hexb*$^{-/-}$*FcRγ*$^{+/+}$ mice, was found to be specifically expressed in the thymus, and B1 cells were also detected at increased levels in the thymus (Fig. 6A, B, 7). High expression of CXCL13 has been found previously in many autoimmune diseases, such as myasthenia gravis [31], multiple sclerosis [33], and in a model mouse of SLE [26], and is considered to be associated with autoantibody production. We have shown also in our previous study that a significant elevation of serum antibody levels occurs in the terminal stages of *Hexb*$^{-/-}$*FcRγ*$^{+/+}$ mice of more than 14 weeks of age [10]. Thus, a high expression of CXCL13 and infiltration of B1 cells in *Hexb*$^{-/-}$*FcRγ*$^{+/+}$ mice may be a reflection of autoantibody production.

Based on our current results, we propose a mechanism by which thymic alterations occur in *Hexb* deficient mice as follows. The apoptosis of immature T cells occurs normally in *Hexb*$^{-/-}$*FcRγ*$^{+/+}$ mice and these apoptotic T cells are engulfed by macrophages. However, macrophages cannot degrade the glycolipids from apoptotic T cells in these animals because of their *Hexb* deficiency, and thus accumulate these molecules in lysosomes. The macrophages are then activated and produce CXCL13, which promotes chemotaxis toward B1 cells and thus leads to the development of autoimmunity. Once autoantibodies against T cells are produced, the storage of T cell-derived glycolipids by macrophages is enhanced via the autoantibody-dependent phagocytosis of T cells.

This undesired loop results in a disrupted immune system and in the production of autoantibodies against neuronal cell antigens or neuronal cell - T cell common antigens such as GA2. Deletion of *FcRγ* may thus prevent thymic involution by blocking the autoantibody dependent phagocytosis of T cells and suppressing specific gene expression. A reduction of the serum titer against GM2 and GA2 in $Hexb^{-/-}FcR\gamma^{-/-}$ mice [10] might be related to thymic integrity. Further studies involving other factors, such as functional testing of single lymphocytes and innate immunity, will be needed to further our understanding of autoimmunity in GM2 gangliosidoses.

Materials and Methods

Animals

All mice used in this study were bred and housed under specific pathogen-free (SPF) conditions. All mouse experiments were approved by the Animal Committee at Yokohama City University. SD model mice ($Hexb^{-/-}$ mice; C57BL/6×129/Sv background) were kindly provided by R. L. Proia (NIH, Bethesda, MD) and were bred in a closed colony over 30 generations to inbreed for C57BL/6- and 129/Sv-derived genes [4]. *FcRγ* gene deficient $Hexb^{-/-}$ mice ($Hexb^{-/-}FcR\gamma^{-/-}$) were generated by described as previously [10]. Each experiment utilized tissue from $Hexb^{+/-}$ $FcR\gamma^{+/+}$, $Hexb^{-/-}FcR\gamma^{+/+}$ and $Hexb^{-/-}$ $FcR\gamma^{-/-}$ mice. All mice were euthanized by inhalation of sevoflurane and the thymus in each case was collected aseptically for further analysis.

Human thymus

A hematoxylin and eosin (H&E) stained slide of a human thymus, dissected from an 11-month-old male with SD who was autopsied at Kobe Children's Hospital [47], was kindly loaned by Dr. H. Itoh.

Histopathology

The mice were perfused with 10% buffered formalin (Sigma-Aldrich Corp. St. Louis, MO) and processed for paraffin embedding. Deparaffinized and rehydrated sections (4 μm) were stained with H&E or used for immunostaining. Apoptosis was detected via the *in situ* terminal deoxy nucleotidyl transferase-mediated dUTP nick end labeling (TUNEL) method using an ApopTag® kit (Millipore, Billerica, MA). For staining ionized calcium binding adaptor molecule 1 (Iba-1), sections were treated with antigen retrieval reagent and then incubated with rabbit anti-Iba-1 antibody (Wako Pure Chemical Industries, Ltd., Osaka, Japan) overnight at 4°C. The washed sections were incubated with biotinylated anti-rabbit IgG antibody (Nichirei, Tokyo, Japan) and subsequently incubated with horseradish peroxidase (HRP) labeled streptavidin (Nichirei). The peroxidase reaction was visualized by diaminobenzidine (DAB) and hydrogen peroxide. For frozen sections, the thymus of each mouse were embedded in OCT compound (Sakura Finetek, Torrance, CA) and quickly frozen in dry ice. For the staining of CXCL13, frozen sections (7 μm) were stained with goat anti-CXCL13 pAb (R&D Systems, Inc., Minneapolis, MN), followed by HRP labeled goat anti-rat IgG (Nichirei). For the staining of CD19, frozen sections (7 μm) were stained with Rat anti-CD19 mAb (6D5; Chemicon International, inc., Temecula, CA), followed by HRP labeled goat anti-rat IgG (Nichirei). For Transmission electron microscopy (TEM), thymic tissues was prefixed with 2.5% glutaraldehyde (Merck & Co., Inc., Whitehouse Station, NJ) and postfixed with 1% osmium tetroxide (Wako Pure Chemical). The samples were embedded in Epon 812 resin (TAAB Laboratories, Aldermaston, Berkshire, UK). Ultra-thin sections were stained with uranyl acetate and lead citrate (Wako Pure Chemical). Samples were observed with an H-7500 electron microscope (Hitachi, Tokyo, Japan).

Flow cytometry

The remaining thymus samples were gently mechanically dispersed into PBS containing 3% fetal bovine serum (staining buffer) and filtered through a BD Falcon™ Cell Strainer (70 μm pore size; BD Biosciences, Franklin, NJ) to produce single cell suspensions and washed twice with staining buffer. Aliquots of 1×10^6 thymic cells were incubated with PE-labeled anti-CD4 (GK1.5; eBioscience, Inc., San Diego, CA) and FITC-conjugated anti-CD8 (53-7.6; eBioscience) mouse monoclonal antibodies (mAbs). For three color staining, thymic cells were stained with PE-labeled anti-B220/CD45R (RA3-6B2; BD Biosciences) and FITC-conjugated anti-CD5 (53-7.3RRH; eBioscience) and PE-Cy5 conjugated CD19 (MB19-1; eBioscience) mAbs. For the staining of thymic macrophages, the thymic cells were stained with anti-Iba1 (Wako Pure Chemical), followed by Alexa Fluor ®-488 labeled anti-rabbit IgG (H+L) (Invitrogen, Carlsbad, CA). For the detection of autoantibody deposition on T cells, thymic cells were stained with Goat anti-mouse IgG (Southern Biotech, Birmingham, AL) followed by Alexa Fluor®-488 labeled Donkey anti-Goat IgG (H+L) (Invitrogen) and PE labeled anti-TCRβ (H57-597; eBioscience). Flow cytometric analysis was carried out using FACScan™ with CELLQuest™ software (BD Biosciences) or with FACS Canto II™ with FACSDiva™ software (BD Biosciences).

cDNA microarray

Pooled thymic RNA samples were obtained from two 15 weeks old $Hexb^{-/-}$ mice and two strain-matched, 15 weeks old $Hexb^{+/-}$ mice. cDNA were synthesized by GeneChip T7-Oligo(dT) Promoter Primer Kit (Affymetrix, Inc, Santa Clara, CA) and TaKaRa cDNA Synthesis Kit (TaKaRa Bio Inc, Shiga, Japan) from 10 μg total RNA. Biotinylated cRNA were synthesized by IVT Labeling Kit (Affymetrix). Following fragmentation, 10 μg of cRNA were hybridized for 16 hr at 45°C on GeneChip Mouse Genome 430 2.0 Array (Affymetrix) containing 45101 unique mouse genes. GeneChips were washed and stained in the Affymetrix Fluidics Station 450. GeneChips were scanned using GeneChip Scanner 3000 7G. Single Array Analysis were calculated by Microarray Suite version 5.0 (MAS5.0) with Affymetrix default setting and global scaling as normalization method. The trimmed mean target intensity of each array was arbitrarily set to 500. Signals were calculated using the One-Step Tukey's Biweight Estimate which yields a robust weighted mean. The signal log ratio was computed using a one-step Tukey's Biweight method by taking a mean of the log ratios of the probe pair intensities across the two arrays. All data is MIAME compliant and that the raw data has been deposited in GEO.

Real-time RT-PCR

Total RNA was purified with TRIzol Reagent (Invitrogen). To determine the high CXCL13-expressing cells, a magnetic cell sorting system was used for the RNA preparation. Briefly, a 1×10^6 thymic cell suspension from 15 week old $Hexb^{-/-}FcR\gamma^{+/+}$ mice was stained with CD11b MicroBeads (Miltenyi Biotec, Bergisch Gladbach, Germany) and separated using an MS Column (Miltenyi Biotec), and a MiniMACS® Separator (Miltenyi Biotec). cDNA was synthesized from total RNA by reverse transcription using a commercial cDNA synthesis kit (TaKaRa Bio Inc). cDNA synthesized from 500 ng of total RNA was used as the template in each reaction. The relative gene expression levels were determined using the SYBR® *Premix Ex Taq*™ II (TaKaRa Bio Inc). The

primer sets for ribosomal protein s18 (Rps18) and tumor necrosis factor-alpha (TNF-α) were obtained from TaKaRa Bio. The primer set for macrophage inflammatory protein-1 alpha (Mip-1α) has been described previously [31]. The primers used to amplify Chemokine (C-X-C motif) ligand 13 (CXCL13) are 5′-TCTCTCCAGGCCACGGTATTCT-3′ (forward, F) and, 5′-ACCATTTGGCACGAGGATTCAC (reverse, R) and for stromal cell-derived factor 1 (SDF-1) are 5′-GAGCCAACGTCAAGCATCTG-3′ (F) and 5′-CGGGTCAATGCACACTTGTC-3′ (R). Rps18 was amplified in each reaction simultaneously as a standard control. The fluorescence changes from each well were monitored using an ABI PRISM® 7500 Sequence Detection System (Perkin Elmer, Inc, Waltham, MA).

Statistical analysis

Statistical analysis was performed using the Student's *t* test. A 95% confidence limit was taken as significant.

Supporting Information

Figure S1 Immunofluorescent analysis of GA2 and thymocyte, for each thymus derived from *Hexb*$^{+/-}$*FcRγ*$^{+/+}$, *Hexb*$^{-/-}$*FcRγ*$^{+/+}$ and *Hexb*$^{-/-}$*FcRγ*$^{-/-}$ mice. Frozen section of the thymus from 15 week old *Hexb*$^{+/-}$*FcRγ*$^{+/+}$, *Hexb*$^{-/-}$*FcRγ*$^{+/+}$ and *Hexb*$^{-/-}$*FcRγ*$^{-/-}$ and 13 week old *Hexb*$^{-/-}$*FcRγ*$^{+/+}$ mice were labeled GA2 with Alexa Fluor®-488, CD4 and CD8 with Alexa Fluor®-594, and nuclear with Hoechst 33258, respectively. Arrows indicate the deposition of GA2 in the cytosol of the CD4/8 negative cells. Scale bar, 20 μm.

Found at: doi:10.1371/journal.pone.0012105.s001 (0.43 MB PDF)

Acknowledgments

We thank Dr. Richard L. Proia for providing the *Hexb*$^{-/-}$ mice, Dr. Toshiyuki Takai for providing the *FcRγ*$^{-/-}$ mice, Dr. Hiroshi Ito for providing the H&E stained human SD autopsy tissue slides, Dr. Masae Tatematsu for personal communications of relevance to this study, and Dr. Haruto Hojo for advice and expertise in performing TEM. We additionally thank Tamiyo Taniguchi, Shizuko Kobayashi and Sayuri Kanaya for their technical and secretarial assistance.

Author Contributions

Conceived and designed the experiments: SK AY SY. Performed the experiments: SK AY KY YK KS NK ME. Analyzed the data: SK AY IA SY. Contributed reagents/materials/analysis tools: KS YN KN YH AR IA. Wrote the paper: SK AY SY.

References

1. Neufeld EF (1991) Lysosomal storage diseases. Annu Rev Biochem 60: 257–280.
2. Gravel RA, Clarke JTR, Kaback MM, Mahuran D, Sandhoff K, et al. (2001) The GM2 gangliosidoses. In: Scriver CR, Beaudet AL, Sly WS, eds. The metabolic and molecular basis of inherited disease. 7th ed. New York: McGraw-Hill. New York. pp 3827–3876.
3. Yamanaka S, Johnson ON, Norflus F, Boles DJ, Proia RL (1994) Structure and expression of the mouse β-hexosaminidase genes, *Hexa* and *Hexb*. Genomics 1994 21: 588–596.
4. Sango K, Yamanaka S, Hoffmann A, Okuda Y, Grinberg A, et al. (1995) Mouse models of Tay-Sachs and Sandhoff diseases differ in neurologic phenotype and ganglioside metabolism. Mice lacking both subunits of lysosomal β-hexosaminidase display gangliosidosis and mucopolysaccharidosis. Nat Genet 11: 170–176.
5. Phaneuf D, Wakamatsu N, Huang J-Q, Borowski A, Peterson AC, et al. (1996) Dramatically different phenotypes in mouse models of human Tay-Sachs and Sandhoff diseases. Hum Mol Genet 5: 1–14.
6. Huang JQ, Trasler JM, Igdoura S, Michaud J, Hanal N, et al. (1997) Apoptotic cell death in mouse models of G_{M2} gangliosidosis and observations on human Tay-Sachs and Sandhoff diseases. Hum Mol Genet 6: 1879–1885.
7. Norflus F, Tifft CJ, McDonald MP, Goldstein G, Crawley JN, et al. (1999) Bone marrow transplantation prolongs life span and ameliorates neurologic manifestations in Sandhoff disease mice. J Clin Invest 101: 1881–1888.
8. Wada R, Tifft CJ, Proia RL (2000) Microglial activation precedes acute neurodegeneration in Sandhoff disease and is suppressed by bone marrow transplantation. Proc Natl Acad Sci USA 97: 10954–10959.
9. Castaneda JA, Lim MJ, Cooper JD, Pearce DA (2008) Immune system irregularities in lysosomal storage disorders. Acta Neuropathol 115: 159–174.
10. Yamaguchi A, Katsuyama K, Nagahama K, Takai T, Aoki I, et al. (2004) Possible role of autoantibodies in the pathophysiology of GM2 gangliosidoses. J Clin Invest 113: 200–208.
11. DiRosario J, Divers E, Wang C, Etter J, Charrier A, et al. (2008) Innate and adaptive immune activation in the brain of MPS IIIB mouse model. J Neurosci Res 87: 978–990.
12. Chattopadhyay S, Ito M, Cooper JD, Brooks AI, Curran TM, et al. (2002) An autoantibody inhibitory to glutamic acid decarboxylase in the neurodegenerative disorder Batten disease. Hum Mol Genet 11: 1421–1431.
13. Lim MJ, Alexander N, Benedict JW, Chattopadhyay S, Shemilt SJA, et al. (2007) IgG entry and deposition are components of the neuroimmune response in Batten disease. Neurobiol Dis 25: 239–251.
14. Ramirez-Montealegre D, Chattopadhyay S, Curran TM, Wasserfall C, Pritchard L, et al. (2005) Autoimmunity to glutamic acid decarboxylase in the neurodegenerative disorder Batten disease. Neurology 64: 743–745.
15. Pearce DA, Atkinson M, Tagle DA (2004) Glutamic acid decarboxylase autoimmunity in Batten disease and other disorders. Neurology 63: 2001–2005.
16. Shoenfeld Y, Beresovski A, Zharhary D, Tomer Y, Swissa M, et al. (1995) Natural autoantibodies in sera of patients with Gaucher's disease. J Clin Immunol 15: 363–372.
17. Balreira A, Lacerda L, Miranda CS, Arosa FA (2005) Evidence for a link between sphingolipid metabolism and expression of CD1d and MHC-class II: monocytes from Gaucher disease patients as a model. Br J Haematol 129: 667–676.
18. Zhou J, Shao H, Cox NR, Baker HJ, Ewald SJ (1998) Gangliosides enhance apoptosis of thymocytes. Cell Immunol 183: 90–98.
19. Cox NR, Ewald SJ, Morrison NE, Gentry AS, Schuler M, et al. (1998) Thymic alterations in feline GM1 gangliosidosis. Vet Immunol Immunopathol 63: 335–353.
20. Zhou J, Cox NR, Ewald SJ, Morrison NE, Basker HJ (1998) Evaluation of GM1 ganglioside-mediated apoptosis in feline thymocytes. Vet Immunol Immunopathol 66: 25–42.
21. Galbiati F, Basso V, Cantuti L, Givogri MI, Lopez-Rosas A, et al. (2007) Autonomic denervation of lymphoid organs leads to epigenetic immune atrophy in a mouse model of Krabbe disease. J Neurosci 27: 13730–13738.
22. Gadola SD, Silk JD, Jeans A, Illarionov PA, Salio M, et al. (2006) Impaired selection of invariant natural killer T cells in diverse mouse models of glycosphingolipid lysosomal storage diseases. J Exp Med 203: 2293–2303.
23. Gerard C, Rollins BJ (2001) Chemokines and disease. Nat Immunol 2: 108–115.
24. Ishikawa S, Sato T, Abe M, Nagai S, Onai N, et al. (2001) Aberrant high expression of B lymphocyte chemokine (BLC/CXCL13) by $CD11b^{+}CD11c^{+}$ dendritic cells in murine lupus and preferential chemotaxis of B1 cells towards BLC. J Exp Med 193: 1393–1402.
25. Sato T, Ishikawa S, Akadegawa K, Ito T, Yurino H, et al. (2004) Aberrant B1 cell migration into the thymus results in activation of CD4 T cells through its potent antigen-presenting activity in the development of murine lupus. Eur J Immunol 34: 3346–3358.
26. Ishikawa S, Matsushima K (2007) Aberrant B1 cell trafficking in a murine model for lupus. Front Biosci 12: 1790–1803.
27. Hayakawa K, Hardy RR, Parks DR, Herzenberg LA (1983) The "Ly-1 B" cell subpopulations in normal, immunodefective, and autoimmune mice. J Exp Med 157: 202–218.
28. Herzenberg LA, Stall AM, Lalor PA, Sidman C, Moore WA, et al. (1986) The Ly-1 B cell lineage. Immunol Rev 93: 81–102.
29. Herzenberg LA (2000) B-1 cells: the lineage question revisited. Immunol Rev 175: 9–22.
30. Wu Y-P, Proia RL (2004) Deletion of macrophage-inflammatory protein 1α retards neurodegeneration in Sandhoff disease mice. Proc Natl Acad Sci U S A 101: 8425–8430.
31. Meraouna A, Cizeron-Clairac G, Panse RL, Bismuth J, Truffault F, et al. (2006) The chemokine CXCL13 is a key molecule in autoimmune myasthenia gravis. Blood 108: 432–440.
32. Ferri C, Colaci M, Battolla L, Giuggioli D, Sebastiani M (2006) Thymus alterations and systemic sclerosis. Rheumatology (Oxford) 45: 72–75.
33. Cavallotti D, D'Andrea V, Pastore FS, Leali FMT, Cavallotti C (2005) Pathogenesis of some neurological immune ultrastructural and morphometrical observations on rat thymus. Neurol Res 27: 41–46.
34. Zhou D, Mattner J, Cantu C, Schrantz N, Yin N, Gao Y, et al. (2004) Lysosomal glycosphingolipid recognition by NKT cells. Science 306: 1786–1789.
35. Takahashi A, Saito K, Koizumi Y (1974) An autopsy case of Sandhoff disease. Beitr Pathol 152: 418–28.

36. Tatematsu M, Imaida K, Ito N, Togari H, Suzuki Y, et al. (1981) Sandhoff disease. Acta Pathol Jpn 31: 503–512.
37. Schwarting GA, Gajewski A (1981) Glycolipids of murine lymphocyte subpopulations: a defect in the levels of sialidase-sensitive sialosylated asialo GM1 in beige mouse lymphocytes. J Immunol 126: 2403–2407.
38. Schwarting GA, Gajewski A (1983) Glycolipids of murine lymphocyte subpopulations. Structural characterization of thymus gangliosides. J Biol Chem 258: 5893–5898.
39. Tsuji D, Kuroki A, Ishibashi Y, Itakura T, Kuwahara J, et al. (2005) Specific induction of macrophage inflammatory protein 1-α in glial cells of Sandhoff disease model mice associated with accumulation of *N*-acetylhexosaminyl glycoconjugates. J Neurochem 92: 1497–1507.
40. Jeyakumar M, Thomas R, Elliot-Smith E, Smith DA, van der Spoel AC, et al. (2003) Central nervous system inflammation is a hallmark of pathogenesis in mouse models of GM1 and GM2 gangliosidosis. Brain 126: 974–987.
41. Kawane K, Ohtani M, Miwa K, Kizawa T, Kanbara Y, et al. (2004) Chronic polyarthritis caused by mammalian DNA that escapes from degradation in macrophages. Nature 443: 998–1002.
42. Halle A, Hornung V, Petzold GC, Stewart CR, Monks BG, et al. (2008) The NALP3 inflammasome is involved in the innate immune response to amyloid-β. Nat Immunol 9: 857–865.
43. Hornung V, Bauernfeind F, Halle A, Samstad EO, Kono H, et al. (2008) Silica crystals and aluminum salts activate the NALP3 inflammasome through phagosomal destabilization. Nat Immunol 9: 847–856.
44. Dostert C, Petrilli V, Van BR, Steele C, Mossman BT, et al. (2008) Innate immune activation through Nalp3 inflammasome sensing of asbestos and silica. Science 320: 674–677.
45. Muruve DA, Petrilli V, Zaiss AK, White LR, Clark SA, et al. (2008) The inflammasome recognizes cytosolic microbial and host DNA and triggers an innate immune response. Nature 452: 103–107.
46. Petrilli V, Dostert C, Muruve DA, Tschopp J (2007) The inflammasome: a danger sensing complex triggering innate immunity. Curr Opin Immunol 19: 615–622.
47. Itoh H, Tanaka J, Morihana Y, Tamaki T (1984) The fine structure of cytoplasmic inclusions in brain and other visceral organs in Sandhoff disease. Brain Dev 6: 467–474.